EUROPEAN ORGANIZATION FOR NUCLEAR RESEARCH (CERN)

CERN-EP-2024-053
2024/03/08

CMS-EXO-22-019

Search for long-lived heavy neutrinos in the decays of B mesons produced in proton-proton collisions at $\sqrt{s} = 13\,\text{TeV}$

The CMS Collaboration*

Abstract

A search for long-lived heavy neutrinos (N) in the decays of B mesons produced in proton-proton collisions at $\sqrt{s} = 13\,\text{TeV}$ is presented. The data sample corresponds to an integrated luminosity of $41.6\,\text{fb}^{-1}$ collected in 2018 by the CMS experiment at the CERN LHC, using a dedicated data stream that enhances the number of recorded events containing B mesons. The search probes heavy neutrinos with masses in the range $1 < m_{\text{N}} < 3\,\text{GeV}$ and decay lengths in the range $10^{-2} < c\tau_{\text{N}} < 10^{4}\,\text{mm}$, where τ_{N} is the N proper mean lifetime. Signal events are defined by the signature $\text{B} \to \ell_{\text{B}}\text{NX}$; $\text{N} \to \ell^{\pm}\pi^{\mp}$, where the leptons ℓ_{B} and ℓ can be either a muon or an electron, provided that at least one of them is a muon. The hadronic recoil system, X, is treated inclusively and is not reconstructed. No significant excess of events over the standard model background is observed in any of the $\ell^{\pm}\pi^{\mp}$ invariant mass distributions. Limits at 95% confidence level on the sum of the squares of the mixing amplitudes between heavy and light neutrinos, $|V_{\text{N}}|^2$, and on $c\tau_{\text{N}}$ are obtained in different mixing scenarios for both Majorana and Dirac-like N particles. The most stringent upper limit $|V_{\text{N}}|^2 < 2.0 \times 10^{-5}$ is obtained at $m_{\text{N}} = 1.95\,\text{GeV}$ for the Majorana case where N mixes exclusively with muon neutrinos. The limits on $|V_{\text{N}}|^2$ for masses $1 < m_{\text{N}} < 1.7\,\text{GeV}$ are the most stringent from a collider experiment to date.

Submitted to the Journal of High Energy Physics

*See Appendix A for the list of collaboration members

1 Introduction

The standard model (SM) of particle physics is a highly predictive and well-tested theoretical framework that describes the electroweak and strong interactions, which together account for the known fundamental forces of nature apart from gravity. Although its predictions are in agreement with a vast number of experimental measurements, performed over a wide range of energies, the SM is unable to provide explanations for many key questions, both observational and theoretical. For example, the minimal SM does not account for the small, but nonzero neutrino masses [1]; for the large amount of dark matter (DM) inferred from astrophysical and cosmological measurements [2]; and for the asymmetry in the abundance of matter and antimatter in the universe [3]. A central challenge of particle physics is therefore to develop and experimentally test new theoretical frameworks that encompass the successful predictions of the SM, but which also provide explanations for physics beyond the SM.

An example of such an extension of the SM is the neutrino minimal standard model (νMSM) [4, 5]. This model predicts the existence of a new type of particle, the heavy neutral lepton (HNL), also referred to as a heavy neutrino, denoted here by N. The dominant component of such a particle has a right-handed chirality and does not have SM gauge couplings, which is why it is often referred to as a sterile neutrino. Its interactions with SM particles arise through the admixture of an SM neutrino. In the scenario in which three heavy neutrinos are predicted, one with a mass in the keV range and the other two with nearly degenerate masses in the GeV range, this model can provide not only a DM candidate [6] but also a possible mechanism for baryogenesis [7], as well as a possible explanation for the smallness of the masses of the SM neutrinos, through the Type I seesaw mechanism [8].

The present search takes as a framework the phenomenology described in Ref. [9]. The underlying assumption is that the N states are not mass degenerate, which implies that they are produced and decay independently, or, alternatively, that their degeneracy is so close that they can be considered a single particle for all practical purposes in this search. This search can be formulated in terms of a single N, parametrized by its mass m_{N} and its mixing amplitudes to the three lepton flavour families, denoted as V_{eN}, $V_{\mu\mathrm{N}}$, and $V_{\tau\mathrm{N}}$. The quantity $|V_{\mathrm{N}}|^2$ is defined as $|V_{\mathrm{N}}|^2 \equiv |V_{\mathrm{eN}}|^2 + |V_{\mu\mathrm{N}}|^2 + |V_{\tau\mathrm{N}}|^2$, and the mixing ratios r_ℓ, with $\ell = (\mathrm{e}, \mu, \tau)$, are defined as $r_\ell \equiv |V_{\ell\mathrm{N}}|^2/|V_{\mathrm{N}}|^2$, with $r_{\mathrm{e}} + r_\mu + r_\tau = 1$ by construction. The proper mean lifetime of the heavy neutrino, τ_{N}, depends on m_{N} and $|V_{\mathrm{N}}|^2$ as $\tau_{\mathrm{N}} \sim |V_{\mathrm{N}}|^{-2} m_{\mathrm{N}}^{-5}$.

Searches for HNLs have been performed by several experiments using a wide range of techniques. Early searches were performed in beam-dump experiments; e.g. the CHARM [10], the NuTeV [11], and the BEBC [12, 13] experiments were sensitive to HNL masses up to about 2 GeV. Searches have been performed by $\mathrm{e^+e^-}$ B-factory experiments, such as Belle [14] and BaBar [15]. At the CERN LHC, limits on heavy neutral leptons have been set by the ATLAS [16, 17], CMS [18–23], and LHCb [24, 25] experiments.

This search probes long-lived N states that can be produced in the leptonic or semileptonic decays of B mesons, through the small admixture of SM neutrinos. A novel and key feature of the analysis is the use of a special b-hadron-enriched sample of proton-proton (pp) collision data, referred to as the B-parking data sample [26], which was collected at a centre-of-mass energy of 13 TeV by the CMS experiment. This data sample corresponds to an integrated luminosity of $41.6\,\mathrm{fb}^{-1}$ and contains of order 10^{10} $\mathrm{b\overline{b}}$ events.

The use of B meson decays as the source of neutrinos provides sensitivity complementary to that of previous CMS HNL searches [18–23], which have exploited on-shell W boson decays

as the source of neutrinos. The B mesons are more abundant in LHC events than W bosons and, because $m_{\mathrm{B}} \ll m_{\mathrm{W}}$, N states produced in B decays generally have lower momenta than those produced in W boson decays. For the long-lived HNLs considered in this search, with $c\tau_{\mathrm{N}}$ ranging from a few microns to a few metres, the softer momentum spectrum leads to a higher fraction of heavy neutrinos decaying within the CMS tracker volume. This volume corresponds to a distance, L_{xy}, in the transverse plane between the HNL decay vertex and the luminous region of $L_{xy} < 1\,\mathrm{m}$.

Heavy neutrinos produced in B meson decays are kinematically constrained to have a mass $m_{\mathrm{N}} \lesssim m_{\mathrm{B}}$, with m_{B} ranging from 5.27 GeV for the lighter $\mathrm{B}^{\pm}$ and B^{0} mesons to 6.25 GeV for the heavier $\mathrm{B}_{\mathrm{c}}^{\pm}$ meson. However, heavy neutrino states with masses below 1 GeV and above 3 GeV are not studied here, as this region of parameter space is well covered by other searches [22, 27]. The B mesons considered for this search are $\mathrm{B}^{\pm}$, B^{0}, $\mathrm{B}_{\mathrm{s}}^{0}$, and $\mathrm{B}_{\mathrm{c}}^{\pm}$, which we denote generically as B_{q} with $\mathrm{q} = (\mathrm{u}, \mathrm{d}, \mathrm{s}, \mathrm{c})$, respectively. Semileptonic b baryon decays are not included in the signal simulation, as their contribution to the expected signal yield is predicted to be significantly smaller than that from B mesons [28]. The production model is discussed in more detail in Section 7, where an explanation is also given of how the extracted signal yields are normalized using the decay $\mathrm{B}^{\pm} \to \mathrm{J}/\psi(1\mathrm{S})(\to \mu^{+}\mu^{-})\mathrm{K}^{\pm}$, which has a similar topology.

The B meson decays considered are either semileptonic (Fig. 1, upper row), producing a lepton, a neutrino, and an accompanying hadronic system, X, or leptonic (Fig. 1, lower row), producing a lepton and a neutrino. The contribution to the expected signal yields of the leptonic channel starts to become relevant for $m_{\mathrm{N}} > 2\,\mathrm{GeV}$. To maximise the signal acceptance, the semileptonic processes are treated inclusively, without attempting to reconstruct the hadronic system X, which can involve complex decay chains. As a consequence, the invariant mass of the B meson is not reconstructed. The charged-lepton candidate from the B meson decay, ℓ_{B}, can either be a muon or an electron. In a signal event, the neutrino flavour eigenstate, $\nu_{\ell_{\mathrm{B}}}$, from the B meson decay chain contains a small admixture of an N mass eigenstate, which subsequently decays via its admixture of the same or another neutrino flavour eigenstate, ν_{ℓ}, into a lepton $\ell^{\pm}$, which is also required to be a muon or an electron, and a charged pion $\pi^{\mp}$. Together, these particles form a neutral $\ell^{\pm}\pi^{\mp}$ system, which can be reconstructed to obtain the invariant mass $m_{\mathrm{N}} = m(\ell^{\pm}\pi^{\mp})$. In the region of parameter space probed here, the HNL is long lived, and its decay gives rise to a displaced vertex (DV), which is a powerful feature of the search signature. Thus, the strategy is defined by three main elements: the $\ell_{\mathrm{B}}(\ell^{\pm}\pi^{\mp})$ event topology, a signal peak in the invariant mass distribution of the $\ell^{\pm}\pi^{\mp}$ system, and a DV associated with the two tracks that form this system. A strength of this analysis is that the mass of the N can be directly probed if a signal is present.

The search is performed under the assumption that N is either a Majorana or a Dirac-like neutrino [29]. For the case in which the N is assumed to be a Majorana particle, the charge of ℓ is not constrained by that of ℓ_{B}, and both opposite-sign (OS) and same-sign (SS) lepton combinations, corresponding to lepton-number-conserving (LNC) and lepton-number-violating (LNV) decays, respectively, are considered. For the case in which two quasi-degenerate Majorana states form a Dirac-like state, their destructive interference cancels the LNV decays, constraining the two leptons to be OS [30].

The event sample used in this analysis was recorded using single muon triggers with relatively low threshold on the muon transverse momentum, p_{T}, as described in Section 3. The search algorithm requires that the trigger muon be part of the signal process, shown in Fig. 1, either as ℓ_{B}, or as ℓ. This muon trigger requirement leads to a classification of events according to the flavour combinations of the leptons: $(\ell_{\mathrm{B}}, \ell) = (\mu\mu, \mathrm{e}\mu, \mu\mathrm{e})$. The $\mu\mu$ channel is referred to

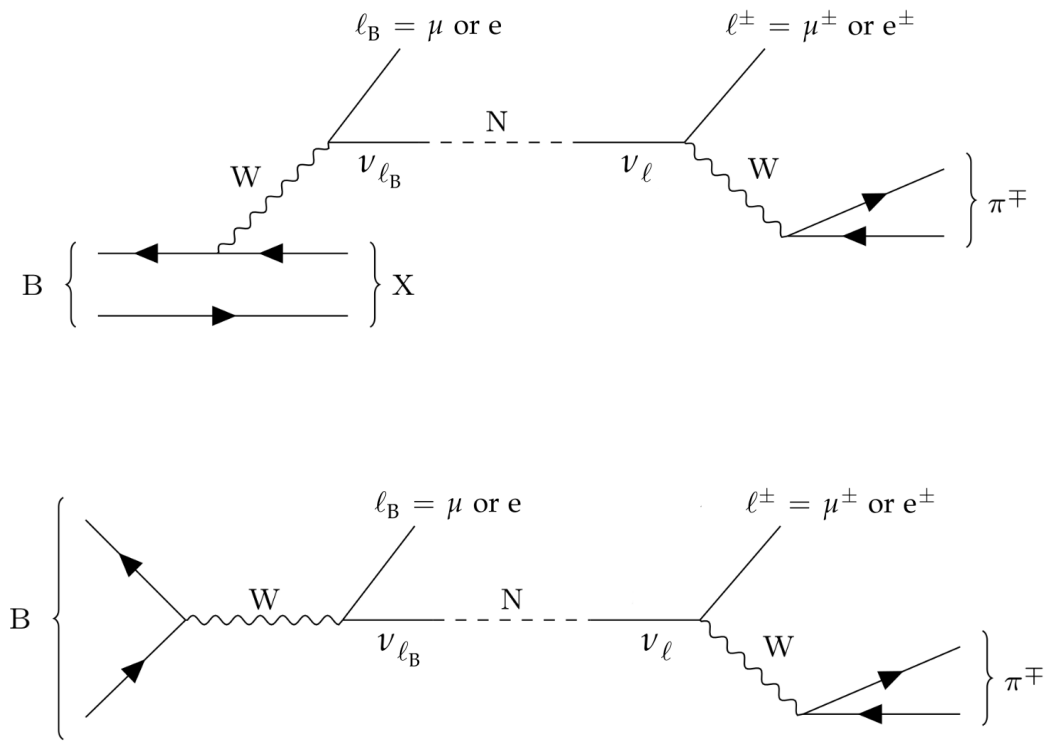

Figure 1: Feynman diagrams showing the semileptonic (upper row) and leptonic (lower row) decay of a B meson into a lepton (ℓ_B), a hadronic system (X) in case of the semileptonic decay, and a neutrino (ν_{ℓ_B}), which contains a small admixture of a heavy neutrino (N). The N mass eigenstate propagates and, according to its admixture of the neutrino flavour eigenstate (ν_ℓ), decays weakly into a lepton $\ell^\pm$ and a charged pion $\pi^\mp$.

as the dimuon channel, while the other two possibilities, i.e. μe and eμ, are referred to as the mixed-flavour channel.

This paper is organised as follows: the CMS detector is described in Section 2, and the data sample is discussed in Section 3, which highlights the role of the special B-parking data stream. The simulated samples, which are only used to model signal events, are described in Section 4. Sections 5 and 6 describe the event reconstruction and selection, respectively. The signal normalization is discussed in Section 7. Section 8 presents the signal extraction method, which is performed using a parametric fit to the data, while Section 9 discusses the systematic uncertainties. The results are presented in Section 10 and are interpreted in the context of the theoretical framework described above. Section 11 summarises the principal results of the paper.

Tabulated results are provided in the HEPData record for this analysis [31].

2 The CMS detector

The central feature of the CMS apparatus is a superconducting solenoid of 6 m internal diameter providing a magnetic field of 3.8 T. Within the solenoid volume are a silicon pixel and strip tracker, a lead tungstate crystal electromagnetic calorimeter (ECAL), and a brass and scintilla-

tor hadron calorimeter (HCAL), each composed of a barrel and two endcap sections. Forward calorimeters extend the pseudorapidity (η) coverage provided by the barrel and endcap detectors. Muons are measured in gas-ionisation detectors embedded in the steel flux-return yoke outside the solenoid. Events of interest are selected using a two-tiered trigger system. The first level (L1), composed of custom hardware processors, uses information from the calorimeters and muon detectors to select events at a rate of around 100 kHz within a fixed latency of 4 μs [32]. The second level, known as the high-level trigger (HLT), consists of a farm of processors running a version of the full event reconstruction software optimized for fast processing, and reduces the event rate to around 1 kHz before data storage [33]. This analysis utilised a special data stream collected at HLT rates up to a few kHz, described in more detail in Section 3. A more detailed description of the CMS detector, together with a definition of the coordinate system used and the relevant kinematic variables, can be found in Ref. [34].

3 The B-parking data sample

The search uses the CMS B-parking data sample [26], which was collected in 2018 using a dedicated data stream to acquire of order 10^{10} $\mathrm{b\bar{b}}$ events, corresponding to an integrated luminosity of 41.6 fb^{-1} [35]. A set of single-muon triggers designed to record events containing B meson semileptonic decays was used. A variety of requirements were placed on the minimum muon p_{T} and the muon transverse impact parameter significance $d_{xy}/\sigma_{d_{xy}}$, where d_{xy} is the transverse impact parameter of the muon with respect to the beam axis and $\sigma_{d_{xy}}$ is its uncertainty. More stringent requirements were in place during higher instantaneous luminosity periods and were progressively relaxed at lower instantaneous luminosities to exploit the spare capacity of the CMS data acquisition system and, therefore, maximise the number of recorded $\mathrm{b\bar{b}}$ events. To maintain good efficiency for muons produced in B decays, the muon p_{T} thresholds were kept low, from 7 to 12 GeV. To control trigger rates, the minimum values used for $d_{xy}/\sigma_{d_{xy}}$ were relatively high, ranging from 3 to 6, thus reducing contamination from prompt muons or muons from charm decays with minimal efficiency penalty for muons from relatively long-lived b hadron decays. Trigger muons were also required to have $|\eta| < 1.5$. The purity of this sample, i.e. the fraction of events containing a $\mathrm{b\bar{b}}$ pair, is approximately 80% [26]. Events in this sample, satisfying the HLT, were collected at a peak rate exceeding 5 kHz, a much higher trigger rate than is normally possible. The sample was stored temporarily in local buffers and then transferred to permanent storage ("parked"), to be processed at the end of the 2018 data-taking period, when computing resources previously allocated otherwise became available.

4 Simulated event samples

Simulated signal event samples are used to design the event selection criteria, to extract the signal shape in the $m(\ell^{\pm}\pi^{\mp})$ distribution used for fitting the data, and to obtain the signal efficiencies as functions of m_{N} and $c\tau_{\mathrm{N}}$. Signal events involve quantum chromodynamics (QCD) production of a b quark-antiquark pair, followed by the fragmentation of these quarks into a variety of B mesons. In the simulation, one of these B mesons undergoes either a semileptonic or a leptonic decay, as shown in Fig. 1, either of which yields an HNL characterised by its mass, m_{N}, and its proper mean lifetime, τ_{N}.

Two sets of signal samples are generated: the first corresponds to N production in the decays of $\mathrm{B_u}$, $\mathrm{B_d}$, and $\mathrm{B_s}$ mesons, while the second corresponds to N production in $\mathrm{B_c}$ meson decays. A dedicated simulation of $\mathrm{B_c}$ decays is required because of its low fragmentation fraction compared to other b hadron species [28, 36]. For the ($\mathrm{B_u}$, $\mathrm{B_d}$, $\mathrm{B_s}$) samples, the pp colli-

sions and hadronisation are simulated with PYTHIA 8.230 [37], using the underlying event tune CP5 [38], the parton distribution functions NNPDF3.1 [39], and the SoftQCD:nonDiffractive process (aimed to inclusively reproduce minimum-bias interactions), while the B meson and N decays are simulated using EVTGEN 1.30 [40], with a phase space decay model (PHSP). For the B_c samples, the pp collisions are first generated with the BCVEGPY 2.2b generator [41], with one B_c meson per event. The events are then passed to PYTHIA and EVTGEN for the hadronisation and signal decay, respectively, in a fashion similar to that used for the (B_u, B_d, B_s) samples. In both cases, the generated events are then propagated through the simulated CMS detector using the GEANT4 package [42] and eventually reconstructed using the standard CMS software. The presence of extra pp collisions within the same or neighbouring bunch crossings (pileup) is taken into account in these event samples by adding simulated minimum bias events. An event weight is applied to correct the underlying pileup distribution to match that observed in the B-parking data, which has an average of about 25 simultaneous collisions per event. In the signal samples, the same triggers used to record the data are simulated. However, the dependence of the trigger thresholds on the instantaneous luminosity present in data, as described in Section 3, is not accounted for in the simulated samples. Therefore, simulated events are weighted to reproduce this effect, using corrections measured in data with the tag-and-probe method [43] and the benchmark $J/\psi(1S) \to \mu\mu$ process. Finally, weights are applied to improve the modelling of the lepton identification algorithm.

Simulated signal event samples are generated with a range of different values of m_N and $c\tau_N$ to span the accessible parameter space in these quantities. By default, the HNL is assumed to be a Majorana fermion, allowing both $N \to \ell^+\pi^-$ and $N \to \ell^-\pi^+$ decays with equal probabilities. As will be discussed in Section 10, these simulated samples can also be used to model the Dirac-like case. Signal samples with $1.0 \leq m_N \leq 3.0\,\text{GeV}$ are simulated with a step size of 20 MeV for masses $1.0 \leq m_N < 1.5\,\text{GeV}$, 30 MeV for masses $1.5 \leq m_N < 2.0\,\text{GeV}$, and 50 MeV for masses $2.0 \leq m_N < 3.0\,\text{GeV}$. This set contains more than 60 signal mass hypotheses. The step size increases with the tested mass to match the detector resolution. For each value of m_N, one to four samples with different $c\tau_N$ hypotheses are generated, with $1 < c\tau_N < 1000\,\text{mm}$. The grid of the values of $c\tau_N$ was chosen to be relatively coarse, because, for each m_N, it is possible to obtain samples of events corresponding to different $c\tau_N$ values by applying an event weight correcting the decay length distribution of the generated sample to a new $c\tau_N$ value. This procedure, referred to hereafter as $c\tau_N$-reweighting, is an important tool in the analysis, as it allows a fine grid of $c\tau_N$ points to be tested.

Simulated background samples are not required, either for the design of the analysis or the signal extraction.

5 Event reconstruction

The event reconstruction identifies candidates for the lepton originating from the B decay (ℓ_B), the displaced lepton ($\ell^\pm$), and the displaced charged pion ($\pi^\mp$). We discuss the criteria used to define each of these reconstructed objects, as well as the procedure used to reconstruct the DV associated with the $\ell^\pm\pi^\mp$ system. At this stage, kinematic and topological selections are applied to ensure the presence of a candidate event in the acceptance. Backgrounds are further suppressed using the multivariate discriminator discussed in Section 6.

Muons are reconstructed from the tracks measured in the silicon tracker system, together with track segments measured in the muon detectors. The candidates must not have significant associated energy deposits in the calorimeters [43]. Muons that satisfy the HLT requirements

for the B-parking data stream are required to have $p_{\mathrm{T}} > 7\,\mathrm{GeV}$ and $|\eta| < 1.5$, while other muons are required to have $p_{\mathrm{T}} > 2\,\mathrm{GeV}$ and $|\eta| < 2$.

The muon candidates originating from the B vertex are required to satisfy the following criteria: the associated track in the silicon tracker must correspond to a high-quality track [44, 45] (at least 5 hits in the silicon tracker and at least 1 hit in the pixel detector), and this track must be matched to at least one muon segment in the muon spectrometer. The track's longitudinal impact parameter, d_z, measured with respect to the primary vertex (PV), defined as the vertex with the largest sum of square of the p_{T} of its tracks, must be less than 20 cm, and its transverse impact parameter, d_{xy}, must be less than 0.3 cm to be consistent with a typical b hadron decay. For displaced muon candidates, a particle-flow reconstruction algorithm [44] is used, and the candidates must satisfy loose displacement criteria: $d_z > 15\,\mu\mathrm{m}$, $d_{xy} > 10\,\mu\mathrm{m}$ and $d_z/\sigma_{d_z} > 1.0$, $d_{xy}/\sigma_{d_{xy}} > 1.5$.

Electrons are reconstructed from energy clusters deposited in the ECAL and the track in the silicon tracker, using a procedure [46] that recovers the energy lost via bremsstrahlung. Electron candidates are required to have $p_{\mathrm{T}} > 1.5\,\mathrm{GeV}$ and to be within the ECAL barrel, i.e. $|\eta| < 1.48$. To improve the selection efficiency of real electrons relative to the background, the electrons, either originating from the B or N vertex, are identified with a multivariate discriminant [46], based on a boosted decision tree (BDT) architecture. The algorithm uses the properties of the reconstructed electron, including the electromagnetic shower shape, the track-cluster matching, the ECAL/HCAL energy ratio, the track quality, and the track impact parameters with respect to the PV. This BDT discriminant, widely used in CMS, was optimized for electrons with transverse momentum greater than 10 GeV; thus it has been retrained to focus on electrons with comparatively lower p_{T}, down to 1.5 GeV, and improve its performance in the context of this analysis [26]. The displaced electrons are further required to satisfy minimal displacement criteria and to have $d_z > 15\,\mu\mathrm{m}$ and $d_{xy} > 10\,\mu\mathrm{m}$, as well as $d_z/\sigma_{d_z} > 1.0$ and $d_{xy}/\sigma_{d_{xy}} > 1.5$.

Displaced pions are reconstructed from high-quality tracks to which the pion mass is assigned. They must have $p_{\mathrm{T}} > 1.0\,\mathrm{GeV}$, $|\eta| < 2$, as well as $d_z > 50\,\mu\mathrm{m}$, $d_{xy} > 50\,\mu\mathrm{m}$, and $d_z/\sigma_{d_z} > 1.5$, $d_{xy}/\sigma_{d_{xy}} > 5.0$.

Given that the HNL is electrically neutral, the charges of the displaced lepton and pion are required to be opposite. A common DV associated with the intersection of the $\ell^{\pm}$ and $\pi^{\mp}$ tracks is computed using a kinematic vertex fit [47], which is based on a least mean square minimization with Lagrange multipliers and Kalman filter techniques. The momenta of the displaced lepton and pion are then recomputed using the DV as a constraint, improving the resolution. The p-value associated with the fit's χ^2 is required to be greater than 0.01.

Since only HNLs decaying into visible particles are considered as signal, the reconstructed transverse momentum $\vec{p}_{\mathrm{T}}$ of the $\ell^{\pm}\pi^{\mp}$ system is aligned with the projection of the direction of flight of the HNL in the transverse plane $\vec{u}_{\mathrm{N}}$. However, the exact HNL direction of flight is not known, as we do not identify the B decay vertex. Nevertheless, given that, in the most relevant part of the tested phase space, the parent B meson travels a significantly shorter distance than an HNL, we assume, with good approximation, that $\vec{u}_{\mathrm{N}}$ is represented by the vector joining the luminous region and the DV. The angle θ between these two vectors $\vec{u}_{\mathrm{N}}$ and $\vec{p}_{\mathrm{T}}$, referred to as the back-pointing angle, peaks at small values and is required to satisfy $\cos\theta > 0.999$. Finally, the significance of the transverse displacement of the DV with respect to the luminous region, $L_{xy}/\sigma_{L_{xy}}$, is required to be greater than 15.

The event reconstruction requirements described above are referred to hereafter as the baseline event selection. This selection consists only of requirements designed to ensure that the two

leptons and the charged pion are well reconstructed, the relative charges of the $\ell^{\pm}\pi^{\mp}$ system are compatible with the signal hypothesis, and the tracks associated with the $\ell^{\pm}\pi^{\mp}$ system are consistent with a common, displaced decay vertex. For simulated signal events, the reconstructed candidates are matched to the generator-level particles, to ensure that the signal candidates are genuine. For moderate decay lengths, background events passing the baseline selection arise primarily from QCD processes, which can lead to cascade decays of B mesons that mimic certain features of the signal signature. In addition, a variety of other combinatorial backgrounds can enter the signal region, and detector reconstruction effects, including particle misidentification, secondary interactions in the tracker material, and pileup, can also play a role.

Figure 2 shows distributions of the key variables $m(\ell^{\pm}\pi^{\mp})$ and $L_{xy}/\sigma_{L_{xy}}$ for events in the dimuon channel in data and in simulated signal samples, after imposing the baseline event selection. Two examples of the corresponding distributions for signal events in simulation are shown. These signals peak sharply at the assumed masses of the N, in this case, $m_{\mathrm{N}} = 1.0$ and 2.0 GeV, as shown in Fig. 2 (left). The distributions of $L_{xy}/\sigma_{L_{xy}}$ are shown in Fig. 2 (right). The data distribution falls with increasing values of $L_{xy}/\sigma_{L_{xy}}$, as expected from its dominant composition of promptly decaying and short-lived particles.

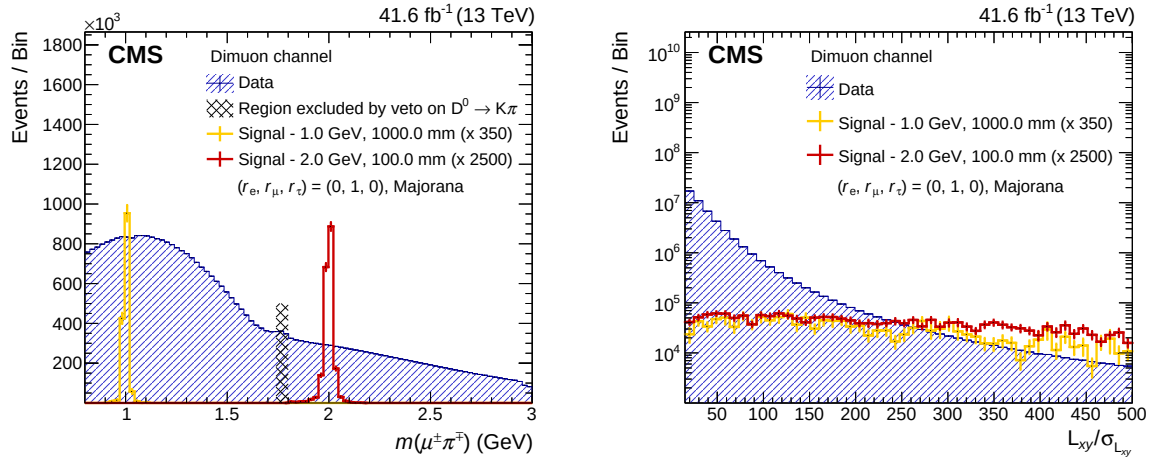

Figure 2: Distribution of the displaced $\mu^{\pm}\pi^{\mp}$ invariant mass (left) and $L_{xy}/\sigma_{L_{xy}}$ (right) in data and in simulated event samples corresponding to two different signal hypotheses, in the Majorana scenario, and with the N mixing exclusively with the muon sector: $m_{\mathrm{N}} = 1\,\mathrm{GeV}$, $c\tau_{\mathrm{N}} = 1000\,\mathrm{mm}$, $|V_{\mathrm{N}}|^2 = |V_{\mu\mathrm{N}}|^2 = 5.4 \times 10^{-4}$; and $m_{\mathrm{N}} = 2\,\mathrm{GeV}$, $c\tau_{\mathrm{N}} = 100\,\mathrm{mm}$, $|V_{\mathrm{N}}|^2 = |V_{\mu\mathrm{N}}|^2 = 1.7 \times 10^{-4}$. The signal distributions are scaled with factors given in the legend. The vertical lines show the statistical uncertainty in each bin.

A number of peaks are observed in the reconstructed invariant mass distributions that are associated with known decay modes of SM particles. The peaks can occur in the two-body systems $\mu_{\mathrm{B}}\mu^{\pm}$, $\mu_{\mathrm{B}}\pi^{\mp}$, and $\mathrm{e}_{\mathrm{B}}\pi^{\mp}$, which sometimes result from particle misidentification. To suppress backgrounds in which such resonances are present, a set of vetoes is applied, as listed in Table 1. The only residual peaking background in the $\ell^{\pm}\pi^{\mp}$ mass spectra consists of the $\mathrm{D}^0 \to \mathrm{K}^{\pm}\pi^{\mp}$ process, where one hadron (typically the kaon) is misidentified as a lepton. Therefore, to avoid the possible contamination from two-body D^0 meson decays, no signal extraction, described in detail in Section 8, is performed between 1.74 and 1.80 GeV. The vetoed region does not centre on the nominal D^0 meson mass owing to mass shift effects related to the final state misidentification.

6 Event categories and selection

After the baseline selection described in Section 5, events are assigned to categories according to (i) three ranges in the significance of the transverse decay length, $L_{xy}/\sigma_{L_{xy}}$, of the $\ell^{\pm}\pi^{\mp}$ system, (ii) two possibilities for the relative sign of the charged leptons, (iii) two ranges in the invariant mass of the $\ell_{\mathrm{B}}\ell^{\pm}\pi^{\mp}$ system, and (iv) the dimuon and mixed-flavour channels introduced in Section 1. Table 2 lists the categories associated with these quantities, as well as the three lepton-flavour categories allowed for the selected $\ell_{\mathrm{B}}\ell$ combinations. Combining these criteria leads to an event classification in terms of 24 mutually exclusive categories. The category based on $L_{xy}/\sigma_{L_{xy}}$ provides a way to increase the sensitivity to different $c\tau_{\mathrm{N}}$ hypotheses. Because the dominant backgrounds arise from promptly or quasi-promptly decaying QCD processes (relative to the N lifetime), the background falls with $L_{xy}/\sigma_{L_{xy}}$, as seen in Fig. 2 (right). The relative sign of the candidate leptons originating from the B and N decay vertex is also a useful quantity for event classification: signal events can contain either SS or OS leptons, while background events are predominantly OS, e.g. B to D cascade decays. Finally, the categorisation in the $\ell_{\mathrm{B}}\ell^{\pm}\pi^{\mp}$ mass provides a way to discriminate signals originating from a $\mathrm{B_u}$, $\mathrm{B_d}$, or $\mathrm{B_s}$ meson from those originating from a $\mathrm{B_c}$ meson. In fact, heavy neutrinos from $\mathrm{B_c}$ mesons are produced almost exclusively through leptonic decays, where all three final state particles, ℓ_{B}, $\ell^{\pm}$, and $\pi^{\mp}$, are reconstructed, allowing the reconstruction of the $\mathrm{B_c}$ invariant mass.

To further improve the sensitivity of the search, a multivariate discriminator is constructed using a wide range of event variables that distinguish statistically between signal and background processes. Because the signal distributions of these variables generally depend on m_{N}, a method is needed to allow the discriminator quantity to incorporate a functional dependence on m_{N}. This capability is provided by a parametric neural network (pNN) [48]. Such a neural network (NN) has, in addition to a set of input variables, $\vec{x}$, a set of discrete parameters, $\vec{\theta}$, and it returns a score that is a function of the full variable set $f\left(\vec{x}, \vec{\theta}\right)$. For this analysis, only a

Table 1: List of considered SM resonances and the corresponding vetoes in the various two-particle invariant mass spectra. The first seven lines consider any possible opposite-sign pair comprising the lepton originating from the B decay and either of the displaced $\ell^{\pm}$ and $\pi^{\mp}$. Events that fail the veto conditions are removed from the analysis. The last two lines pertain to the displaced $\ell^{\pm}\pi^{\mp}$ candidate and indicate that the signal extraction is not performed and exclusion limits are not provided for m_{N} in the vetoed regions. The presence of misidentified particles is also indicated. For the $\mathrm{D^0}$ meson vetoes, the mass range is adjusted to account for the incorrect mass hypothesis assigned to the misidentified particle.

Mass spectrum	Process	Veto (GeV)	Categories	Misidentification
$m(\mu_{\mathrm{B}}\mu^{\pm})$	$\phi(1020) \to \mu\mu$	$\lvert m(\mu_{\mathrm{B}}\mu^{\pm}) - 1.02\rvert > 0.01$	OS	0
	$\mathrm{J}/\psi(1\mathrm{S}) \to \mu\mu$	$\lvert m(\mu_{\mathrm{B}}\mu^{\pm}) - 3.10\rvert > 0.15$	OS	0
	$\psi(2\mathrm{S}) \to \mu\mu$	$\lvert m(\mu_{\mathrm{B}}\mu^{\pm}) - 3.69\rvert > 0.08$	OS	0
$m(\mu_{\mathrm{B}}\pi^{\mp})$	$\mathrm{J}/\psi(1\mathrm{S}) \to \mu\mu$	$\lvert m(\mu_{\mathrm{B}}\pi^{\mp}) - 3.10\rvert > 0.05$	SS	1 misid. π
	$\mathrm{D^0} \to \mathrm{K}\pi$	$\lvert m(\mu_{\mathrm{B}}\pi^{\mp}) - 1.76\rvert > 0.05$	SS	1 misid. μ
$m(\mathrm{e}_{\mathrm{B}}\pi^{\mp})$	$\mathrm{J}/\psi(1\mathrm{S}) \to \mathrm{ee}$	$\lvert m(\mathrm{e}_{\mathrm{B}}\pi^{\mp}) - 3.10\rvert > 0.05$	SS	1 misid. π
	$\mathrm{D^0} \to \mathrm{K}\pi$	$\lvert m(\mathrm{e}_{p}\pi^{\mp}) - 1.76\rvert > 0.05$	SS	1 misid. e
$m(\mu^{\pm}\pi^{\mp})$	$\mathrm{D^0} \to \mathrm{K}\pi$	$\lvert m(\mu^{\pm}\pi^{\mp}) - 1.77\rvert > 0.03$	all	1 misid. μ
$m(\mathrm{e}^{\pm}\pi^{\mp})$	$\mathrm{D^0} \to \mathrm{K}\pi$	$\lvert m(\mathrm{e}^{\pm}\pi^{\mp}) - 1.77\rvert > 0.03$	all	1 misid. e

Table 2: Summary of the event categorisation. The events are classified into 24 mutually exclusive categories.

Quantity	Label	Definition
$L_{xy}/\sigma_{L_{xy}}$	low $L_{xy}/\sigma_{L_{xy}}$	$L_{xy}/\sigma_{L_{xy}} < 50$
	medium $L_{xy}/\sigma_{L_{xy}}$	$50 < L_{xy}/\sigma_{L_{xy}} < 150$
	high $L_{xy}/\sigma_{L_{xy}}$	$L_{xy}/\sigma_{L_{xy}} > 150$
Relative lepton sign	OS	ℓ_B charge $\neq \ell$ charge
	SS	ℓ_B charge = ℓ charge
$\ell_B\ell^\pm\pi^\mp$ mass	low $\ell_B\ell^\pm\pi^\mp$ mass	$\ell_B\ell^\pm\pi^\mp$ mass $< 5.7\,\text{GeV}$
	high $\ell_B\ell^\pm\pi^\mp$ mass	$\ell_B\ell^\pm\pi^\mp$ mass $> 5.7\,\text{GeV}$
Flavour channel	dimuon	$\ell_B\ell = \mu\mu$
	mixed-flavour	$\ell_B\ell = (\mu\text{e}, \text{e}\mu)$

single parameter, m_N, is used. By incorporating m_N as a parameter, the need for separate trainings for different values of m_N (more than 60 in this analysis) is avoided, and the pNN behaves smoothly for mass values between those used in the training sample. The mass parameters chosen for the training are $m_N = 1.0$, 1.5, 2.0, and 3.0 GeV for both signal and background. The signal signatures also depend on the value of $c\tau_N$. However, this variable is not used as an additional parameter of the pNN, as it was found that training the pNN separately in the different categories of $L_{xy}/\sigma_{L_{xy}}$ ensures good performance for all of the $c\tau_N$ hypotheses.

The pNN is trained separately in each of the categories defined in Table 2. The baseline event selection described in Section 5 is applied to all training samples. The simulated signal event samples for $m_N = 1.0$, 1.5, 2.0, and 3.0 GeV are aggregated into a common signal training sample in which the discrete m_N values are provided to the pNN as a parameter. Because simulating the large cross section background processes is too resource intensive, the background training sample is taken from data but comprises less than one thousandth of all the available data events. The contamination from a hypothetical N signal in such a limited data set would be negligible. To properly train the pNN, it is important to ensure that, for each value of the parameter m_N, the events in the background sample have kinematic properties that correspond to the background events in the $m(\ell^\pm\pi^\mp)$ invariant mass region near m_N. Therefore, selected background events lie within a $\pm 10\sigma$ window around the m_N mass peak, where σ is the mass resolution obtained in the reconstruction of the simulated signal events.

The pNN is trained using input variables that provide a good discrimination between signal and background. These variables, which are discussed in more detail below, are

1. Transverse momenta: $p_T(\ell_B)$, $p_T(\ell^\pm)$, $p_T(\pi^\mp)$.
2. Invariant-masses: $m(\ell_B\pi^\mp)$, $m(\ell_B\ell^\pm)$, $m(\ell_B\ell^\pm\pi^\mp)$.
3. Track separation in the η-φ space (where φ is the azimuthal angle), $\Delta R \equiv \sqrt{(\Delta\eta)^2 + (\Delta\varphi)^2}$: $\Delta R(\ell_B, \ell^\pm)$, $\Delta R(\ell_B, \pi^\mp)$.
4. Displaced vertex properties: $\cos\theta$, fit p-value.
5. Displacement-related quantities: $L_{xy}/\sigma_{L_{xy}}$ and $d_{xy}/\sigma_{d_{xy}}$ of the pion.
6. Track-related information: number of layers of the CMS silicon pixel and strip tracker traversed by the lepton(s) and pion from the DV.

7. Lepton isolation, defined in a cone of ΔR smaller than 0.3 around the lepton momentum vector [43, 46].

Comparisons of signal and background distributions for some of these variables are given in Fig. 3, for representative signals (i) in the dimuon channel, with $m_{\mathrm{N}} = 2\,\mathrm{GeV}$ and $c\tau_{\mathrm{N}} = 100\,\mathrm{mm}$ and (ii) in the category with high $L_{xy}/\sigma_{L_{xy}}$, OS, and low $\ell_{\mathrm{B}}\ell^{\pm}\pi^{\mp}$ mass. Because the p_{T} distribution of the background is typically softer than that of the signal, as can be seen in Fig. 3 (upper left) for the displaced pion, the transverse momentum of the three particles in the final state is added to the variable set. The separation power offered by these quantities depends on the value of m_{N}. For example, the p_{T} of the displaced particles $\ell^{\pm}$ and $\pi^{\mp}$ gets harder as m_{N} gets larger, offering even greater discrimination between the signal and the background.

The set of discriminating variables listed above includes the invariant masses $m(\ell_{\mathrm{B}}\ell^{\pm})$, $m(\ell_{\mathrm{B}}\pi^{\mp})$, and $m(\ell_{\mathrm{B}}\ell^{\pm}\pi^{\mp})$. Figure 3 (upper right) shows the distribution of $m(\ell_{\mathrm{B}}\ell^{\pm}\pi^{\mp})$. For lower values of m_{N}, the B meson decays predominantly via semileptonic processes, while for large values, the semileptonic decay rate falls rapidly and the leptonic rate becomes dominant. In the case where B decays via a semileptonic process, $m(\ell_{\mathrm{B}}\ell^{\pm}\pi^{\mp})$ does not peak at the mass of the B meson, m_{B}, as the accompanying hadronic system X, introduced in Section 1, is not reconstructed. In the leptonic case, a peak at m_{B} is observed, which provides further background rejection.

Because the momenta of the HNL's decay products typically have similar directions in the laboratory frame, the pNN is also trained on the track separation in η-ϕ space, $\Delta R(\ell_{\mathrm{B}}, \ell^{\pm})$, and $\Delta R(\ell_{\mathrm{B}}, \pi^{\mp})$. The quantity $\Delta R(\ell^{\pm}, \pi^{\mp})$ is not added to the training variable set, as, otherwise, the signal mass m_{N} could be learned by the pNN during training because of the addition of the transverse momenta.

The pNN uses two quantities that characterise the N decay vertex, providing additional sensitivity to the $c\tau_{\mathrm{N}}$ hypothesis within each bin of $L_{xy}/\sigma_{L_{xy}}$. These quantities are $\cos\theta$, where θ is the back-pointing angle defined in Section 5, and the DV fit p-value. Figure 3 (lower left) shows signal and background distributions of the quantity $\cos\theta$, which typically peaks at 1 more steeply for signal than for background. As shown in the list above, the pNN is also trained on the $L_{xy}/\sigma_{L_{xy}}$ and the $d_{xy}/\sigma_{d_{xy}}$ of the pion. The distribution of the latter quantity is shown in Fig. 3 (lower right), in which we can see that the long-lived signal reaches larger values compared to the background.

Because the signal is a long-lived particle, additional information on the tracks is provided to the pNN. In particular, the number of layers in the silicon pixel and strip tracker traversed by the charged particles provides good signal-to-background discrimination. Larger values of $c\tau_{\mathrm{N}}$ typically correspond to fewer tracker layers traversed by the daughter lepton and charged pion from the N decay. Finally, the lepton isolation is added to the training variable set, as leptons in a signal event tend to be more isolated than leptons in a background event. This quantity is defined, for both the muon and the electron, as the energy sum of the charged and neutral particles lying in a cone within a distance $\Delta R = 0.3$ from the lepton, from which the contribution from pileup particles is subtracted.

For each mass hypothesis, m_{N}, the pNN score can be interpreted as the probability for an event to originate from a signal with mass m_{N}. This quantity is therefore used to enhance the signal significance with respect to the background. In each mass window, introduced in Section 8, and in each category, listed in Table 2, the events are selected by requiring the pNN score to be greater than 0.99. To avoid the introduction of unintentional biases, this threshold was optimised without viewing the complete data sample.

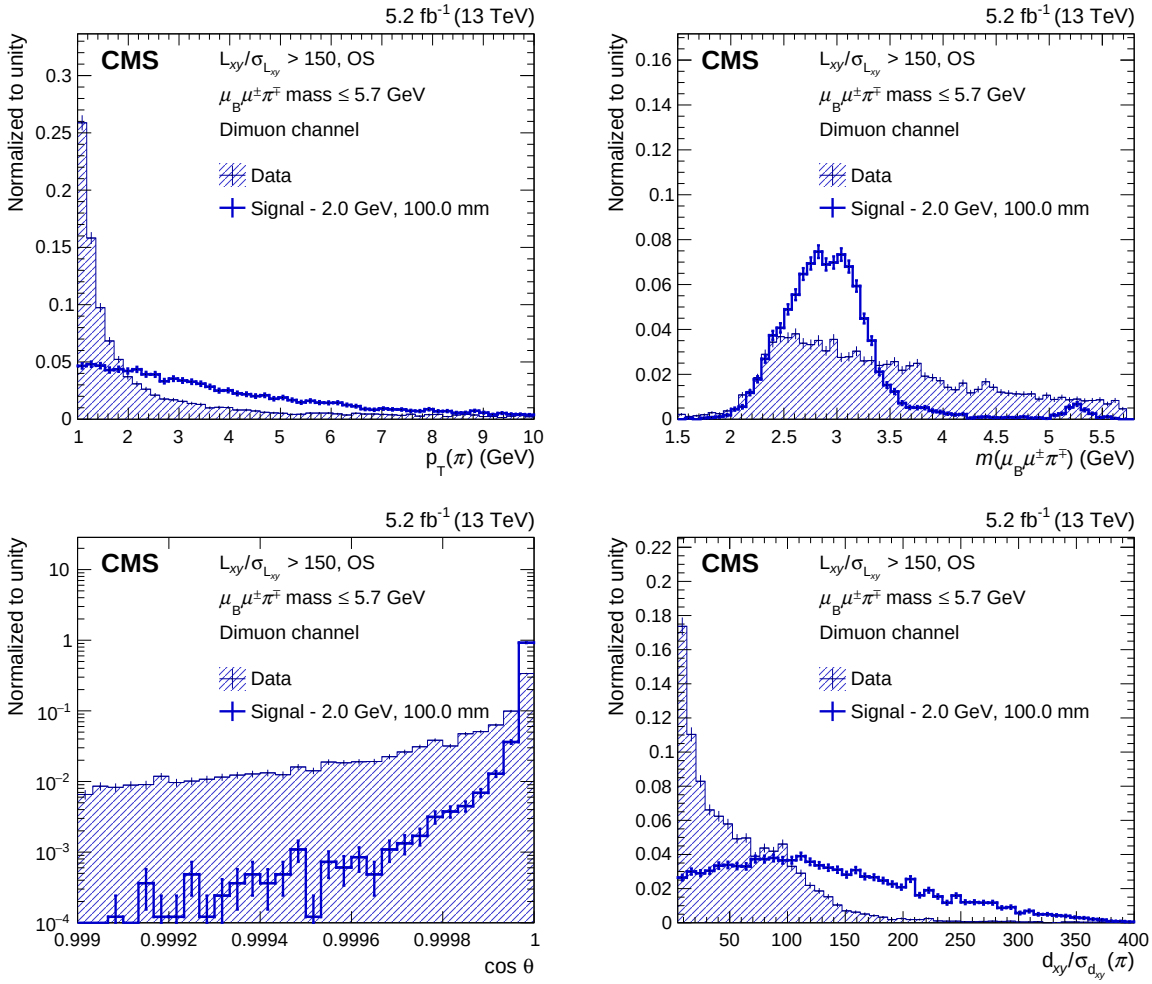

Figure 3: The distributions of the pion p_{T} (upper left), $m(\mu_{\mathrm{B}}\mu^{\pm}\pi^{\mp})$ (upper right), $\cos\theta$ (lower left), and pion $d_{xy}/\sigma_{d_{xy}}$ (lower right) are shown for data, as well as for a signal hypothesis of $m_{\mathrm{N}} = 2\,\mathrm{GeV}$ and $c\tau_{\mathrm{N}} = 100\,\mathrm{mm}$. The data correspond to an integrated luminosity of $5.2\,\mathrm{fb}^{-1}$ and are selected in the mass window of size 10σ around $m_{\mathrm{N}} = 2\,\mathrm{GeV}$. The distributions, which are normalized to unit area, are shown for the dimuon channel in category with high $L_{xy}/\sigma_{L_{xy}}$, OS, and low $\ell_{\mathrm{B}}\ell^{\pm}\pi^{\mp}$ mass. The vertical lines show the statistical uncertainty in each bin.

The pNN architecture is that of a fully connected NN with three layers:

1. Input layer: contains as many nodes as the number of input features, plus one extra node for the mass parameter m_{N}.
2. Hidden layer: contains 64 nodes and is activated by the rectified linear unit (ReLU) function [49, 50], defined as $\mathrm{ReLU}(x) = \max(0, x)$, with $x \in \mathbb{R}$.
3. Output layer: returns the pNN score, normalized to unity through the sigmoid activation function.

The training is performed using the TensorFlow package [51], with the Keras interface [50] and the Adam optimiser [52]. The training aims at minimising the cross-entropy loss function, and the weights are updated using batch gradient descent. The batch size is chosen to

be 32 and the initial learning rate to be 0.01. The input features are normalized using the RobustScaler [53] before the training.

The performance of the pNN is quantified using the area under the ROC curve (AUC), as shown, for example, in Fig. 4 (left) for events in the dimuon channel, and in the category with medium $L_{xy}/\sigma_{L_{xy}}$, OS, and low $\ell_B\ell^\pm\pi^\mp$ mass. The AUC is given as a function of the signal mass for different $c\tau_N$ hypotheses. The large values of the AUC show that the pNN performs well for the various signal hypotheses. The pNN performs well for a wide range of $c\tau_N$ values, with marginal degradation for signals with a smaller decay length.

To validate the use of pNNs instead of regular NNs trained for specific masses, we compare the AUC values obtained for the two approaches. The results of this study are summarised in Fig. 4 (right) for events in the dimuon channel, in the medium $L_{xy}/\sigma_{L_{xy}}$, OS, and low $\ell_B\ell^\pm\pi^\mp$ mass category. The first set of AUC values shown corresponds to the pNN described above and trained on signal masses of $m_N = 1.0$, 1.5, 2.0, and 3.0 GeV. The second set of AUC values was obtained using a NN with the same architecture and training conditions as the pNN, but instead trained only on the mass $m_N = 2$ GeV sample. The different points have $c\tau_N = 10$ mm and are obtained from a corresponding simulated sample, without the use of the $c\tau_N$-reweighting procedure introduced in Section 4. We conclude that the pNN and NN yield the same AUC score for $m_N = 2$ GeV, the common mass they are trained on. Furthermore, the pNN performance remains approximately constant for masses lying between those used for the training, in contrast to the performance loss of the NN for masses other than $m_N = 2$ GeV.

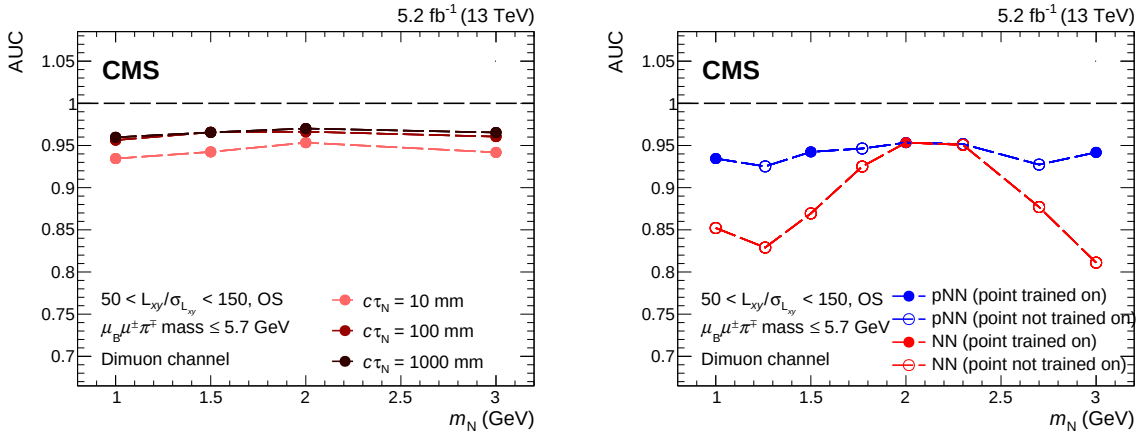

Figure 4: (Left) Performance of the pNN as a function of signal mass for events in the $50 < L_{xy}/\sigma_{L_{xy}} < 150$, OS, and low $\ell_B\ell^\pm\pi^\mp$ mass category in the dimuon channel. The performance is shown by the AUC curve, where a value at unity corresponds to a perfect separation between signal and background. The different coloured curves correspond to different $c\tau_N$ hypotheses. (Right) Validation of the use of a pNN for intermediate m_N mass points, for events in the $50 < L_{xy}/\sigma_{L_{xy}} < 150$, OS and low $\ell_B\ell^\pm\pi^\mp$ mass category in the dimuon channel: a pNN trained on masses $m_N = 1.0$, 1.5, 2.0, and 3.0 GeV (blue) and a NN trained on mass $m_N = 2$ GeV (red). All the points have $c\tau_N = 10$ mm. The full circles correspond to mass points on which the pNN and NN were trained on, while the open circles show mass points that have not been trained on.

7 Signal normalization

The number of expected signal events, N_{sig}, in the flavour channel $\ell_{\text{B}}\ell = (\mu\mu, \text{e}\mu, \mu\text{e})$, for a given N hypothesis specified by m_{N} and $c\tau_{\text{N}}$, and mixing scenario specified by $\vec{r} = (r_{\text{e}}, r_{\mu}, r_{\tau})$, is given by

$$N_{\text{sig}}\left(\ell_{\text{B}}\ell, m_{\text{N}}, c\tau_{\text{N}}, \vec{r}\right) = \frac{\sigma^{\text{eff}}_{\text{B}^{\pm}}}{f_u}\mathcal{L}\sum_{\text{q}} F^{\text{q}}_{\text{N}}\left(\ell_{\text{B}}\ell, m_{\text{N}}, c\tau_{\text{N}}, \vec{r}\right)\epsilon^{\text{q}}_{\text{sig}}\left(\ell_{\text{B}}\ell, m_{\text{N}}, c\tau_{\text{N}}\right), \tag{1}$$

where $\sigma^{\text{eff}}_{\text{B}^{\pm}}$ is the effective total cross section for both B^{+} and B^{-} meson production, extrapolated from the measured fiducial cross section of the process $\text{B}^{\pm} \to \text{J}/\psi(1\text{S})(\to \mu^{+}\mu^{-})\text{K}^{\pm}$ in the phase space covered by the trigger conditions described in Section 3; f_u is the fragmentation fraction of the charged B meson B_{u}; $\mathcal{L}$ is the integrated luminosity for the B-parking data sample; the quark flavour index, q, runs over (u, d, s, c); F^{q}_{N} is the product of the N production rate and decay branching fractions associated with a signal originating from the decay of a meson B_{q}; and $\epsilon^{\text{q}}_{\text{sig}}$ is the associated signal efficiency, incorporating the acceptance, reconstruction, trigger, and selection efficiencies. The signal factor, F^{q}_{N}, in Eq. (1) is defined as

$$F^{\text{q}}_{\text{N}}\left(\ell_{\text{B}}\ell, m_{\text{N}}, c\tau_{\text{N}}, \vec{r}\right) = \underbrace{\sum_{\text{X}_{\text{b}}} f_{\text{q}}\frac{\widetilde{\Gamma}(\text{B}_{\text{q}} \to \ell_{\text{B}}\text{NX}_{\text{b}})}{\Gamma(\text{B}_{\text{q}})} r_{\ell_{\text{B}}}|V_{\text{N}}|^2}_{\text{N production}} \underbrace{\frac{\widetilde{\Gamma}(\text{N} \to \ell\pi)}{r_{\text{e}}\widetilde{\Gamma}_{\text{e}}(\text{N}) + r_{\mu}\widetilde{\Gamma}_{\mu}(\text{N}) + r_{\tau}\widetilde{\Gamma}_{\tau}(\text{N})} r_{\ell}}_{\text{N decay}}. \tag{2}$$

In the N production term, the sum runs over the possible hadronic systems, X_{b}, associated with the decay of the meson B_{q}; f_{q} is the fragmentation fraction of the meson B_{q}; $\Gamma(\text{B}_{\text{q}})$ is the SM B_{q} decay width [28]; and $\widetilde{\Gamma}(\text{B}_{\text{q}} \to \ell_{\text{B}}\text{NX}_{\text{b}})$ is the partial decay rate for inclusive production of the N with lepton of flavour ℓ_{B} (as computed from Ref. [9]) divided by $|V_{\ell_{\text{B}}\text{N}}|^2$, which is factored out and written explicitly as $r_{\ell_{\text{B}}}|V_{\text{N}}|^2$. In the N decay term, the factor $\widetilde{\Gamma}(\text{N} \to \ell\pi)$ is the partial decay width with $|V_{\ell\text{N}}|^2$ factored out, and $\widetilde{\Gamma}_{\alpha}(\text{N})$ is the total decay width for an N decaying into a charged or neutral lepton of flavour $\alpha = (\text{e}, \mu, \tau)$, with $|V_{\alpha\text{N}}|^2$ factored out. In the ratio between $|V_{\ell\text{N}}|^2$ and $|V_{\alpha\text{N}}|^2$, the factor $|V_{\text{N}}|^2$ cancels out, leaving the mixing ratio r_{ℓ}, in the numerator, and the mixing ratios, r_{α}, in the denominator. The N decay widths are computed based on Ref. [9].

The quantities $|V_{\text{N}}|^2$, $c\tau_{\text{N}}$, and $\vec{r}$ are linked to each other by the following relation:

$$\frac{1}{c\tau_{\text{N}}} = |V_{\text{N}}|^2\left(r_{\text{e}}\widetilde{\Gamma}_{\text{e}}(\text{N}) + r_{\mu}\widetilde{\Gamma}_{\mu}(\text{N}) + r_{\tau}\widetilde{\Gamma}_{\tau}(\text{N})\right), \tag{3}$$

which implies that different combinations of $\vec{r}$ and $|V_{\text{N}}|^2$ yield the same N lifetime $c\tau_{\text{N}}$. This property underpins the interpretations of the results in various flavour mixing, as well as in the Majorana or Dirac-like scenarios, discussed in Section 10.

The decay branching fractions multiplied by the fragmentation fractions, f_{q}, for the four B meson species are shown in Fig. 5 as a function of m_{N} for the scenario in which N can only couple to muons. For masses approaching $m_{\text{N}} = 3\,\text{GeV}$, the B_{c} meson contribution becomes significant, despite its low fragmentation fraction, because of the predominance of leptonic decays and the larger B_{c} mass. For smaller masses, the dominant contribution is from the B_{u}, B_{d}, and B_{s} mesons. The branching fractions for the process $\text{N} \to \mu^{\pm}\pi^{\mp}$ range from 22% down

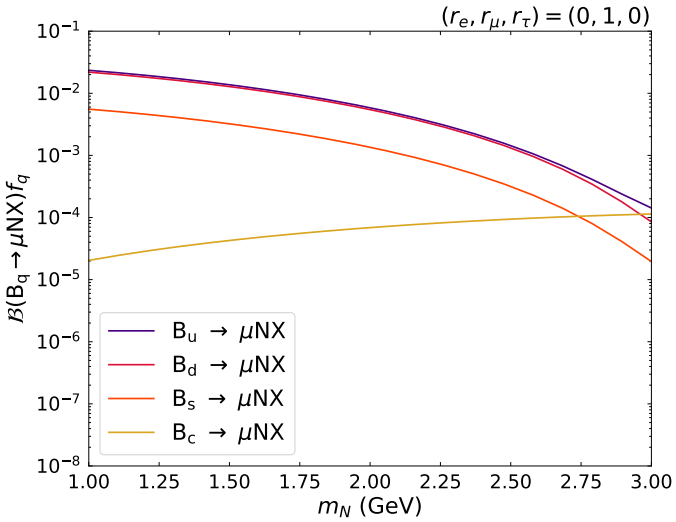

Figure 5: Branching fractions as functions of m_{N} for $\mathrm{B_q} \to \mu\mathrm{NX}$ decays, $\mathrm{q} = (\mathrm{u}, \mathrm{d}, \mathrm{s}, \mathrm{c})$, multiplied by the corresponding fragmentation fraction, f_{q}. Both leptonic and semileptonic decays are considered. The results are shown for the mixing scenario $|V_{\mathrm{N}}|^2 = |V_{\mu\mathrm{N}}|^2 = 1$. The branching fractions are computed based on the method described in Ref. [9].

to 2.4% for m_{N} masses from 1.0 to 3.0 GeV, respectively, in the scenario where the N couples exclusively to muons.

The total effective cross section, $\sigma^{\mathrm{eff}}_{\mathrm{B}^\pm}$, is extrapolated from the measurement of the cross section for the SM control process $\mathrm{B}^\pm \to \mathrm{J}/\psi(1\mathrm{S})(\to \mu^+\mu^-)\mathrm{K}^\pm$, performed in the fiducial phase space imposed by the trigger requirements of the B-parking sample, discussed in Section 3. In particular, the leading muon must have $p_{\mathrm{T}} > 7$ GeV and $|\eta| < 1.5$. We note that a similar measurement has already been performed by CMS, within a defined fiducial phase space [54]. In a manner similar to Eq. (1), the expected number of control events is computed as the product of the cross section, $\sigma^{\mathrm{eff}}_{\mathrm{B}^\pm}$; the relevant SM branching fractions; the integrated luminosity; and the efficiency of the SM decay, accounting for the acceptance, selection, and trigger effects. The efficiency is obtained from a simulation of the control process. The associated sample is simulated using the same generator conditions as for the signal samples described in Section 4, such that the measurement of $\sigma^{\mathrm{eff}}_{\mathrm{B}^\pm}$ using the control process can be extrapolated to the signal process. The cross section $\sigma^{\mathrm{eff}}_{\mathrm{B}^\pm}$ is then obtained by measuring the number of control events in data. The event yield is extracted from the data using an extended unbinned maximum likelihood fit, shown in Fig. 6. The total fit accounts for three components: (i) the signal peak, (ii) the background arising from misreconstructed b hadron decays, such as $\mathrm{B} \to \mathrm{J}/\psi(1\mathrm{S}) + \text{hadrons}$ (partially reconstructed background), and (iii) the background originating from a spurious combination of a $\mathrm{J}/\psi(1\mathrm{S})$ meson and an uncorrelated track (combinatorial background). The sample used for this purpose has an integrated luminosity of $0.77\,\mathrm{fb}^{-1}$, a fraction of that of the full event sample. However, the statistical uncertainty in the yield for the control process is much smaller than the systematic uncertainty (discussed in Section 9). No theoretical uncertainty for the PYTHIA model used for the extrapolation is considered here, since the fiducial phase space selected in this ancillary measurement is close to that covered by the signal in the analysis, such that this uncertainty cancels out in the signal normalization procedure. The measured value is $\sigma^{\mathrm{eff}}_{\mathrm{B}^\pm} = (572.0 \pm 4.9\,(\mathrm{stat}) \pm 85.8\,(\mathrm{syst}))\,\mu\mathrm{b}$.

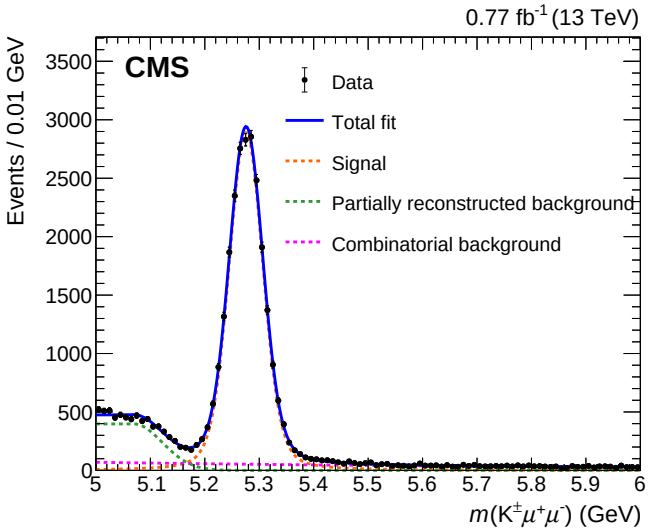

Figure 6: Distribution of the $K^{\pm}\mu^{+}\mu^{-}$ invariant mass for a luminosity of $0.77\,fb^{-1}$. A large signal is observed at the B_u mass. The blue curve shows the fit to signal plus background, while the orange, green, and red curves show the contributions from the signal, composite background, and combinatorial background, respectively.

8 Signal extraction

The signal event yield for each heavy-neutrino mass hypothesis, m_N, is extracted from a simultaneous parametric fit to the $m(\ell^{\pm}\pi^{\mp})$ distributions in data in the different categories listed in Table 2. The baseline selections, the 2-body resonance vetoes listed in Table 1, and the requirement on the pNN score to be greater than 0.99 are all applied before these fits are performed. Because m_N is not predicted and can assume any value allowed by the kinematics of the decays under study in this analysis, we perform the fits to the data in a series of sliding $m(\ell^{\pm}\pi^{\mp})$ mass windows centred around a set of closely spaced trial mass values. The separation of these trial values is about twice the mass resolution, σ, and the window around each trial mass value is $\pm 10\sigma$. The values of σ range approximately from 9 MeV to 25 MeV for signal masses of 1.0 and 3.0 GeV, respectively.

The sum of signal plus background models is fitted to the mass distributions. The signal mass shape is parametrized, in all the categories, and for all N hypotheses, with a double-sided Crystal Ball function [55, 56]. While the parameters describing the power-law tails of the function are fixed, the signal mass resolution, σ, increases linearly with the signal mass m_N.

As anticipated in Section 5, the background is generally falling; however, its shape is not known a priori, and it is allowed to vary in the different mass windows and categories. The background shape is studied prior to the final fit in the sidebands, defined as the regions outside the signal window of size $\pm 3\sigma$ around the mass hypothesis m_N. The parameters controlling the background shapes used in the fit are free-floating and are treated as uncorrelated for the 24 categories and the different mass windows.

To account for possible background shape variations, the discrete profiling method [57] is used. This method employs a set of alternative background shape functions in each mass window and category. The method also provides a way to incorporate a systematic uncertainty associated with the choice of functional form for the background shape by treating this choice as a discrete nuisance parameter (NP). During the fit, at each point of the scan over the signal

strength, the profile-likelihood is evaluated for each function indexed by NP and the best fit one is chosen. The final set of functions considered consists of three families: power-law polynomials, Laurent-series polynomials, and a sum of exponentials. Initially, each family contemplates all functions of any order N.

To avoid overfitting, the maximum order, N_{max}, of the function that is considered in each family, in the sense that a higher order function would not improve the fit, is assessed using a Fisher test [58]. To determine the value of N_{max} for a given family of functions, successive orders are tested iteratively. If the function at order N provides an adequate fit, or N is the lowest order, the function of order $N+1$ is tested by computing $\Delta\text{NLL} = 2(\text{NLL}_N - \text{NLL}_{N+1})$, with NLL_N being the negative log-likelihood of the fit with the function of order N. According to Wilk's theorem [59], ΔNLL behaves asymptotically as a χ^2 with one degree of freedom, allowing one to compute the associated p-value of the test as $p^{\text{F}} = \text{p}(\chi^2 > \Delta\text{NLL})$. If $p^{\text{F}} < 0.05$, the function of order $N+1$ is supported by the data, and the same test will be run for the next-order function. If not, then the testing stops and $N_{\text{max}} = N+1$. For each family, the functional form of order N_{max} is directly added to the final set of functions, as well as the functions with lower order, provided that their associated χ^2-goodness of fit probability exceeds 0.01.

Figure 7 shows an example of a background-only fit in a mass window around 1.5 GeV, in the high $L_{xy}/\sigma_{L_{xy}}$, OS, and low $\ell_{\text{B}}\ell^{\pm}\pi^{\mp}$ mass category in the dimuon channel. The functional form of the background is the one in the set returned as having the best χ^2-goodness of fit. The invariant mass distribution expected for a representative signal is overlaid.

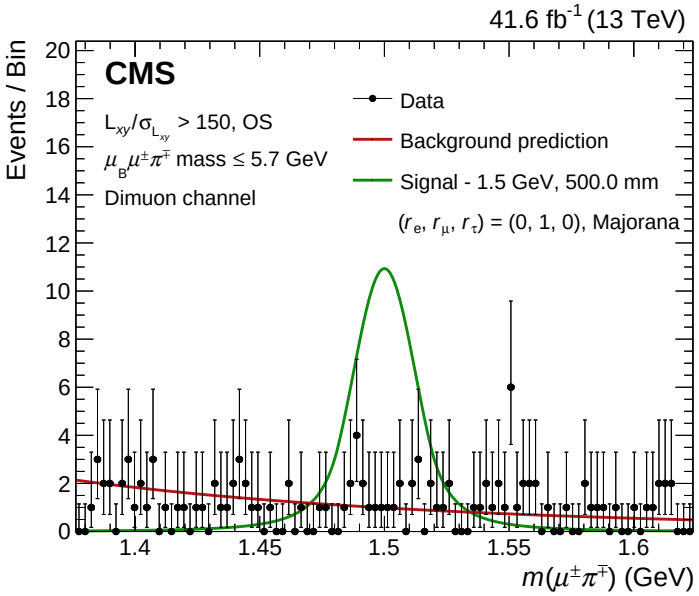

Figure 7: Distribution of the $\mu^{\pm}\pi^{\mp}$ invariant mass in the mass window around 1.5 GeV in the high $L_{xy}/\sigma_{L_{xy}}$, OS, and low $\ell_{\text{B}}\ell^{\pm}\pi^{\mp}$ mass category in the dimuon channel. The result of the background-only fit to the data (red) is shown together with the mass distribution expected from a Majorana signal with $m_{\text{N}} = 1.5$ GeV and $c\tau_{\text{N}} = 500$ mm, for the case in which the N mixes with the muon sector only (green).

9 Systematic uncertainties

The systematic uncertainty in the signal event yield due to the modelling of the background is assessed using the discrete profiling method in the signal extraction, as described in Section 8.

All of the other uncertainties are summarised in Table 3 and are associated with the shape parametrization of the signal invariant mass and the normalization of the signal event yield. These uncertainties are discussed below and are small compared to the uncertainties arising from the size of the event sample or from the fit procedure.

The first source of systematic uncertainty listed in Table 3 is associated with parametrization of the shape of the signal invariant mass distribution. As discussed in Section 8, the signal mass distribution is parametrized using a double-sided Crystal Ball function. In each flavour channel, the parameters of the power-law tails are fixed and the resolution is parametrized linearly in the signal mass, while being treated inclusively between the different $c\tau_{\mathrm{N}}$ hypotheses; the flavour channels; and the categories in $L_{xy}/\sigma_{L_{xy}}$, relative lepton sign, and $\ell_{\mathrm{B}}\ell^{\pm}\pi^{\mp}$ mass. A systematic uncertainty of 15%, obtained by studying the relative change on the median expected limit when varying some of the fit parameters, is applied to account for the possible effects of the choice of signal parametrization. While all the resolution and parameters of the tails are fixed in the final fit, the mean of the distribution has a freedom of 0.1% and 2% for the dimuon and mixed-flavour signals, respectively, to account for the lepton energy uncertainties.

The other systematic uncertainties listed in Table 3 are associated with how the signal event yield is related to the theoretical parameters of interest, as obtained in Eq. (1). The main sources of systematic uncertainty in the determination of the effective $\mathrm{B}^{\pm}$ cross section, $\sigma^{\mathrm{eff}}_{\mathrm{B}^{\pm}}$, (discussed in Section 7) arise from the choice of the model used in the likelihood fits, the reconstruction of the B meson decay vertex, and the muon trigger. These contributions amount to a total uncertainty of 15% in $\sigma^{\mathrm{eff}}_{\mathrm{B}^{\pm}}$. Signal events from $\mathrm{B_c}$ decays (in the high $\ell_{\mathrm{B}}\ell^{\pm}\pi^{\mp}$ mass categories) are subject to an additional uncertainty of 24% in the f_{c} fragmentation because of the currently limited experimental accuracy of the f_{c} measurement [36]. The remaining uncertainties listed in Table 3 are associated with the signal efficiency, $\epsilon^{\mathrm{q}}_{\mathrm{sig}}$. These are

- Uncertainty in the signal efficiency arising from the pNN selection. To estimate this uncertainty, we consider the control process $\mathrm{B}^{\pm} \to \mathrm{J}/\psi(1\mathrm{S})(\to \mu^+\mu^-)\mathrm{K}^{\pm}$. This selection, described in Section 6, is applied in both data and simulation. The residual difference between the pNN output score distribution between data and simulation is taken as the systematic uncertainty. It ranges between 5 and 20%, depending on the event category and it is assigned equally to the dimuon and the mixed-flavour channels, as the pNN is flavour agnostic.
- Uncertainty associated with the matching, described in Section 5, between a reconstructed signal candidate and the underlying generated signal candidate. This uncertainty is 5%.
- Uncertainty in the signal efficiency arising from potential mismodelling of tracking- and vertexing-related quantities that affect measurements of the decay vertices. These are accounted for with a systematic uncertainty of 5%, based on Ref. [21].
- Uncertainties in the signal efficiency arising from correction factors applied to the simulated signal event samples. Several types of such scale factors are applied to improve the agreement between the actual and simulated behavior of the detector, including efficiency scale factors for electrons, muons, and the trigger. The uncertainties in the corrections are 5% and 1% for the trigger and lepton identification scale factors, respectively. These uncertainties are computed by varying the respective scale factor weights up and down by 1 standard deviation and studying the impact on the number of expected signal events. Lepton scale factors are computed using a tag-and-probe method [43].

The systematic uncertainties discussed above are modelled as log-normal uncertainties. Apart from the uncertainty in $\sigma^{\text{eff}}_{\text{B}^\pm}$ and f_{c}, the uncertainties are treated as uncorrelated across the different analysis categories.

Finally, the statistical uncertainty associated with the limited size of the simulated signal samples and the per-event $c\tau_{\text{N}}$-reweighting is taken into account. These uncertainties are assumed to be described by Γ distributions.

Table 3: Sources of systematic uncertainty affecting the expected signal event yield. The ranges given correspond to the uncertainties across the different event categories. The uncertainty in the integrated luminosity is not reported as it is incorporated in the uncertainty in the cross section measurement used to normalize the signal.

Source	Value (%)
Signal shape	15
$\sigma^{\text{eff}}_{\text{B}^\pm}$	15
f_{c}	24
Signal selection	5–20
Limited simulated signal sample size	<15
Matching	5
Tracking efficiency	5
Trigger scale factors	5
Muon identification scale factors	1
Electron identification scale factors	3
Total	<42

10 Results and interpretation

For each mass window around a given signal mass hypothesis, m_{N}, the signal yield is extracted from the data using the procedure explained in Section 8 using the uncertainties summarised in Section 9. No significant excesses over the background-only expectations are observed. As an example, Fig. 8 shows the $\ell^\pm\pi^\mp$ invariant mass distributions in the dimuon channel for the high $L_{xy}/\sigma_{L_{xy}}$, OS, and low $\ell_{\text{B}}\ell^\pm\pi^\mp$ mass category; the mass windows shown are centred around $m_{\text{N}} = 1.0$, 1.5, 2.0, and 2.5 GeV. For these four mass windows, the figure shows the corresponding fits to the data assuming signal hypotheses for the cases $c\tau_{\text{N}} = 10000.0$, 2000.0, 700.0, and 100.0 mm, respectively. These values are close to the exclusion limit when the HNL mixes exclusively with the muon sector, which is the scenario with the greatest sensitivity.

For each value of m_{N}, the results are interpreted using Eqs. (1) and (2), which relate the observed number of signal events, N_{sig}, to the quantity $|V_{\text{N}}|^2$. Upper limits on the signal yields at the 95% confidence level (CL) are used to establish corresponding limits on the quantity $|V_{\text{N}}|^2$, assuming a variety of different mixing scenarios specified by the ratios (r_{e}, r_μ, r_τ) at a fixed proper mean lifetime τ_{N}. These limits are obtained with the combination of the different event categories listed in Table 2. For each signal hypothesis (m_{N}, $c\tau_{\text{N}}$) and each mixing scenario, an unbinned maximum likelihood function, $\mathcal{L}(r, \vec{\theta})$, is constructed using the signal strength, r, as the parameter of interest and the full set of NPs, $\vec{\theta}$, that account for the different sources of uncertainty.

The limits are derived using the CL_s criterion [60] in the asymptotic approximation [61]. A given signal hypothesis is considered to be excluded if a signal strength equal to (or larger

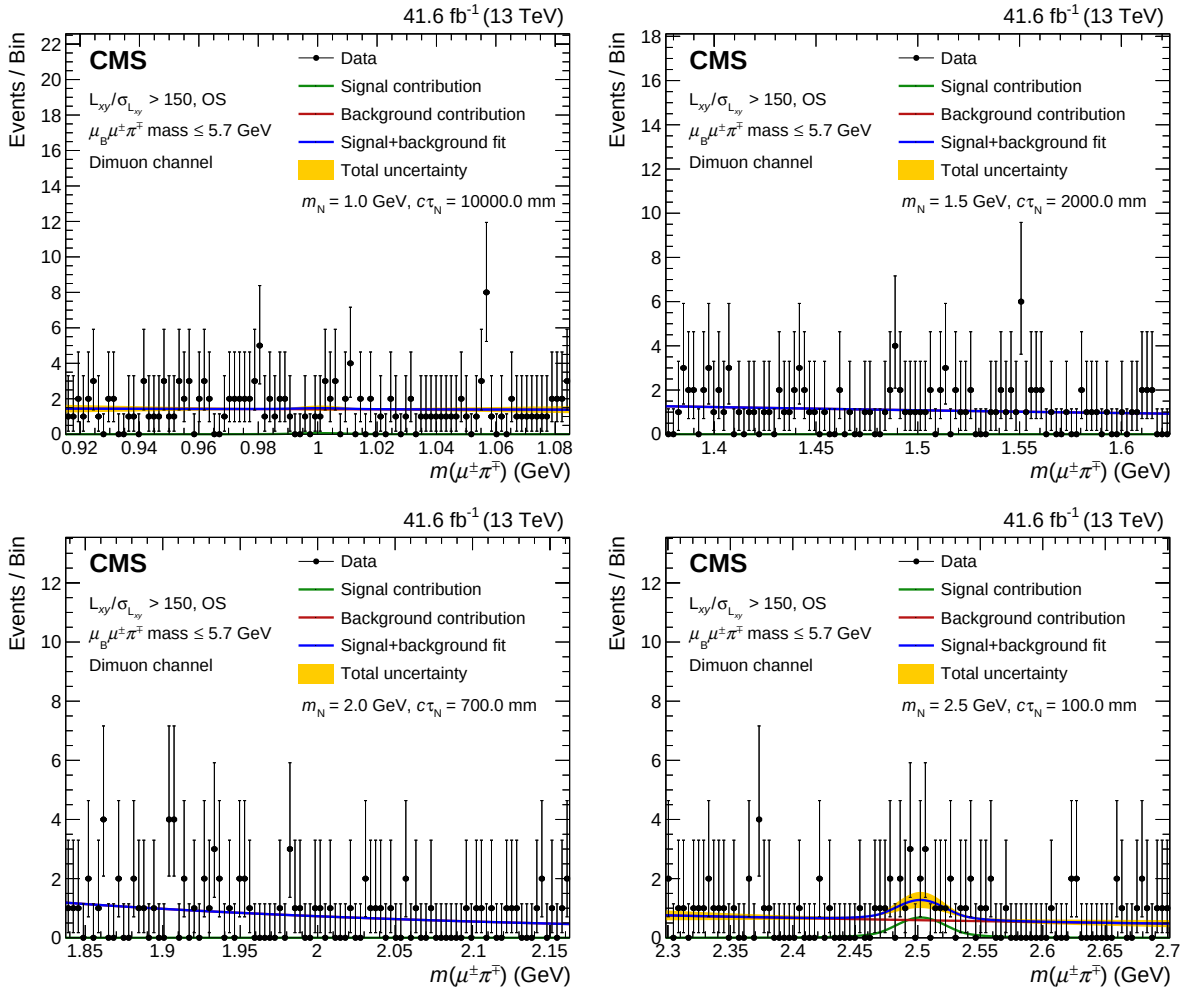

Figure 8: Fits of the mass distribution for a signal of mass $m_{\mathrm{N}} = 1.0\,\mathrm{GeV}$ (upper left), 1.5 GeV (upper right), 2.0 GeV (lower left), and 2.5 GeV (lower right), in the high $L_{xy}/\sigma_{L_{xy}}$, OS, and low $\ell_{\mathrm{B}}\ell^{\pm}\pi^{\mp}$ mass category of the dimuon channel. The blue curve corresponds to signal-plus-background fit, while the green and red curves indicate its individual signal and background components, respectively. The yellow band shows the total post-fit systematic plus statistical uncertainty.

than) unity is not compatible with the observed data at 95% CL. A scan of $|V_{\mathrm{N}}|^2$ on a fine grid is performed using the $c\tau_{\mathrm{N}}$-reweighting methodology described in Section 4.

Limits are derived for both the Majorana and Dirac-like nature of the HNL. As discussed in Section 4, the signal simulation samples are generated for the Majorana case. In the Dirac-like scenario, lepton flavour is conserved, and only OS $\ell_{\mathrm{B}}^{\pm}\ell^{\mp}$ pairs are allowed in the signal process. In the OS categories, for a given m_{N} and $c\tau_{\mathrm{N}}$ point, the expected event yield for the Dirac-like scenario can be obtained from that of the Majorana scenario considering the fact that the decay widths of a Dirac-like N are half of those of a Majorana N [9], resulting in twice the yields in the former case than in the latter. Finally, another consequence of the change of the decay widths is that, for a given m_{N} and $c\tau_{\mathrm{N}}$ hypothesis, the $|V_{\mathrm{N}}|^2$ in the Dirac-like scenario is twice as large as in the Majorana scenario.

The upper exclusion limits on $|V_{\mathrm{N}}|^2$ as a function of the N mass are shown in Figs. 9 and 10, for the Majorana and Dirac-like cases, respectively. In each figure, four benchmark scenarios,

chosen based on the proposal in Ref. [62], are considered: two mixing scenarios derived with the dimuon channel only, with $(r_e, r_\mu, r_\tau) = (0, 1, 0)$ and $(r_e, r_\mu, r_\tau) = (0, 1/2, 1/2)$; and two mixing scenarios derived with the dimuon and mixed-flavour channels combined, namely $(r_e, r_\mu, r_\tau) = (1/2, 1/2, 0)$ and $(r_e, r_\mu, r_\tau) = (1/3, 1/3, 1/3)$. Using Eqs. (2) and (3) and a reweighting procedure, we can obtain exclusion limits for an arbitrary mixing scenario.

The best limit on $|V_N|^2$ is obtained for the muon exclusive mixing scenario $(r_e, r_\mu, r_\tau) = (0, 1, 0)$. This limit excludes at 95% CL values of $|V_N|^2 > 2.0 \times 10^{-5}$ for a signal mass $m_N = 1.95\,\text{GeV}$ for the Majorana case, and $|V_N|^2 > 3.2 \times 10^{-5}$ for a signal mass $m_N = 1.68\,\text{GeV}$ for the Dirac-like case. The best limits on $|V_N|^2$ for the other scenarios are summarised in Table 4.

Table 4: Summary of the most stringent upper limits on $|V_N|^2$ at 95% CL. For each scenario, the minimum excluded value of $|V_N|^2$ is reported together with the mass at which it occurs.

(r_e, r_μ, r_τ)	Scenario	$\lvert V_N\rvert^2$	Mass (GeV)
(0, 1, 0)	Majorana	2.0×10^{-5}	1.95
(0, 1/2, 1/2)	Majorana	4.0×10^{-5}	1.42
(1/2, 1/2, 0)	Majorana	3.3×10^{-5}	2.15
(1/3, 1/3, 1/3)	Majorana	5.0×10^{-5}	2.15
(0, 1, 0)	Dirac-like	3.2×10^{-5}	1.68
(0, 1/2, 1/2)	Dirac-like	6.5×10^{-5}	1.68
(1/2, 1/2, 0)	Dirac-like	5.7×10^{-5}	1.68
(1/3, 1/3, 1/3)	Dirac-like	8.5×10^{-5}	1.68

The muon-exclusive mixing scenario allows a direct comparison with the results from previous work. Compared to results of the ATLAS [17] and CMS [21] Collaborations, targeting long-lived HNLs produced in the decays of W bosons, and analysing $139\,\text{fb}^{-1}$ and $138\,\text{fb}^{-1}$ of data, respectively, the limits are improved by up to a factor of about 3 for masses below 1.75 GeV for the Majorana case, and a factor of about 2 for masses below 1.7 GeV for the Dirac-like case. Furthermore, in the Majorana case, a direct comparison with results from the LHCb [24] (and revised in Ref. [63]) and Belle [14] Collaborations, both targeting the same signal process as in the present search, is possible. Compared to the LHCb search, the limits are improved by up to one order of magnitude, while compared to the Belle results, the limits are improved by up to a factor of about 2 for all masses. Compared to other recent results from CMS [22, 23], this analysis extends and improves the exclusion limits by up to a factor of about 2 in the mass region between 1 and 2 GeV.

The sensitivity for the three other mixing scenarios, with $r_\mu \neq 1$, is less than in the muon exclusive mixing scenario, as the reconstruction efficiency for the muon is greater than that of the electron with CMS.

The observed lower limits at 95% CL on $c\tau_N$ for 66 different mixing scenarios (r_e, r_μ, r_τ), for three values of masses, $m_N = 1.0$, 1.5, and 2.0 GeV, are shown in Fig. 11 for the Majorana and Dirac-like cases. The constraint $r_e + r_\mu + r_\tau = 1$ allows the values to be shown in the form of ternary plots. We verify that the limits improve with increasing values of r_μ, while they slightly degrade with increasing values of r_e. The latter trend is explained by smaller values of $\widetilde{\Gamma}_\tau$ with respect to $\widetilde{\Gamma}_\mu$ and $\widetilde{\Gamma}_e$ in Eq. (3). The best limits on $c\tau_N$ are obtained for a signal mass $m_N = 1\,\text{GeV}$ for the mixing scenario $(r_e, r_\mu, r_\tau) = (0, 1, 0)$. Values of $c\tau_N < 9.2\,\text{m}$ and $c\tau_N < 10.5\,\text{m}$ are excluded at 95% CL for the Majorana and Dirac-like cases, respectively. The most stringent limits on $c\tau_N$ for the all masses are summarised in Table 5 for the Majorana and Dirac-like hypotheses. Unlike the limits obtained on $|V_N|^2$ discussed above, the limits on $c\tau_N$

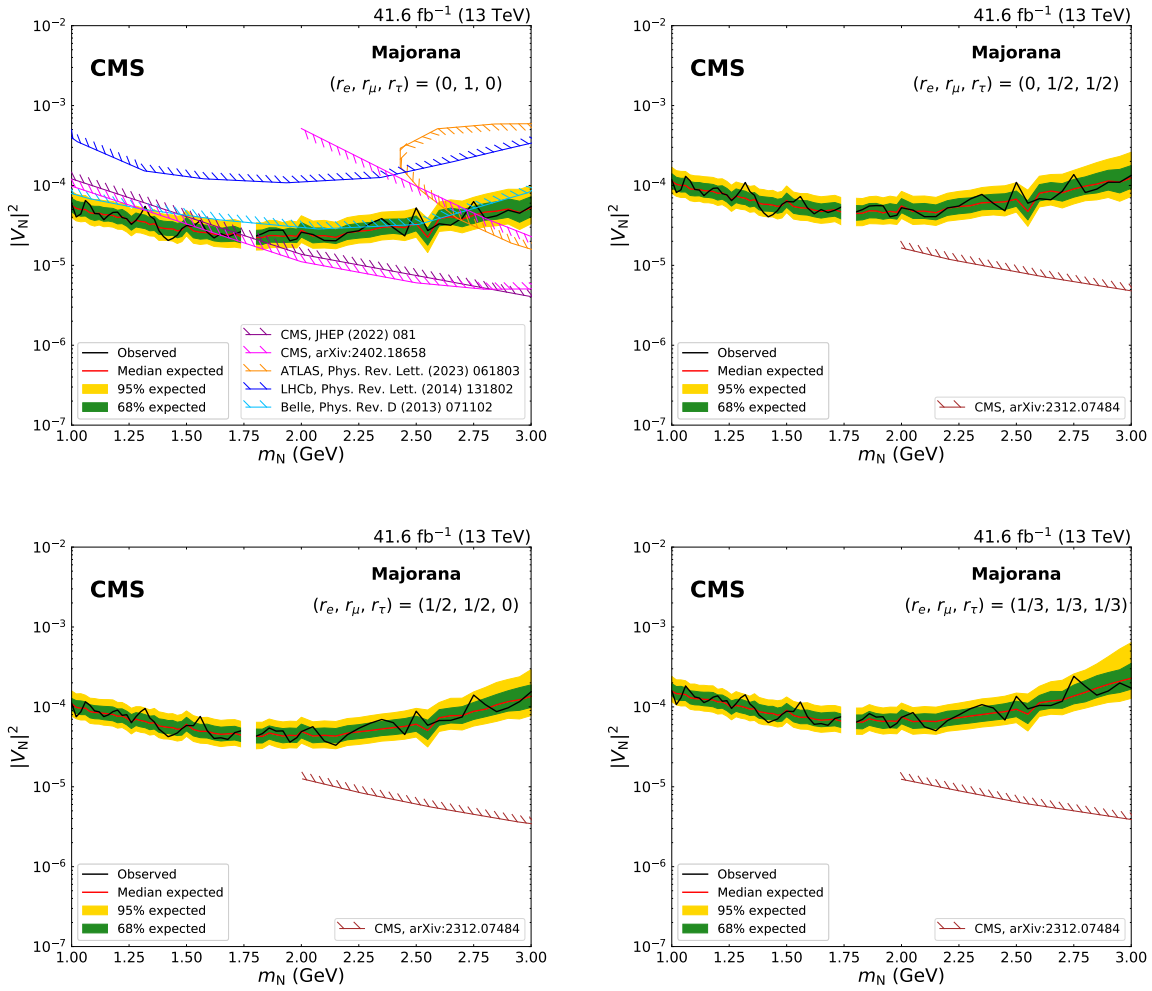

Figure 9: Expected and observed 95% CL limits on $|V_N|^2$ as a function of m_N, in the Majorana scenario. On the upper row, the limits are derived uniquely with the dimuon channel, and are shown for the mixing scenarios $(r_e, r_\mu, r_\tau) = (0, 1, 0)$ on the left and for $(r_e, r_\mu, r_\tau) = (0, 1/2, 1/2)$ on the right; on the lower row, the limits are obtained with the dimuon and mixed-flavour channel combined, for the mixing scenarios $(r_e, r_\mu, r_\tau) = (1/2, 1/2, 0)$ on the left and for $(r_e, r_\mu, r_\tau) = (1/3, 1/3, 1/3)$ on the right. In the upper left figure, results from the CMS [21, 23], ATLAS [17], LHCb [24], and Belle [14] Collaborations are shown as a comparison; in the other figures, results from the CMS Collaboration [22] are reported. The mass range with no results shown corresponds to the D^0 meson veto listed in the lower part of Table 1.

are more stringent in the Dirac-like scenario than in the Majorana scenario. This behaviour is a consequence of $\widetilde{\Gamma}_e$, $\widetilde{\Gamma}_\mu$, and $\widetilde{\Gamma}_\tau$ in Eq. (3) being twice as low in the Dirac-like case as in the Majorana case.

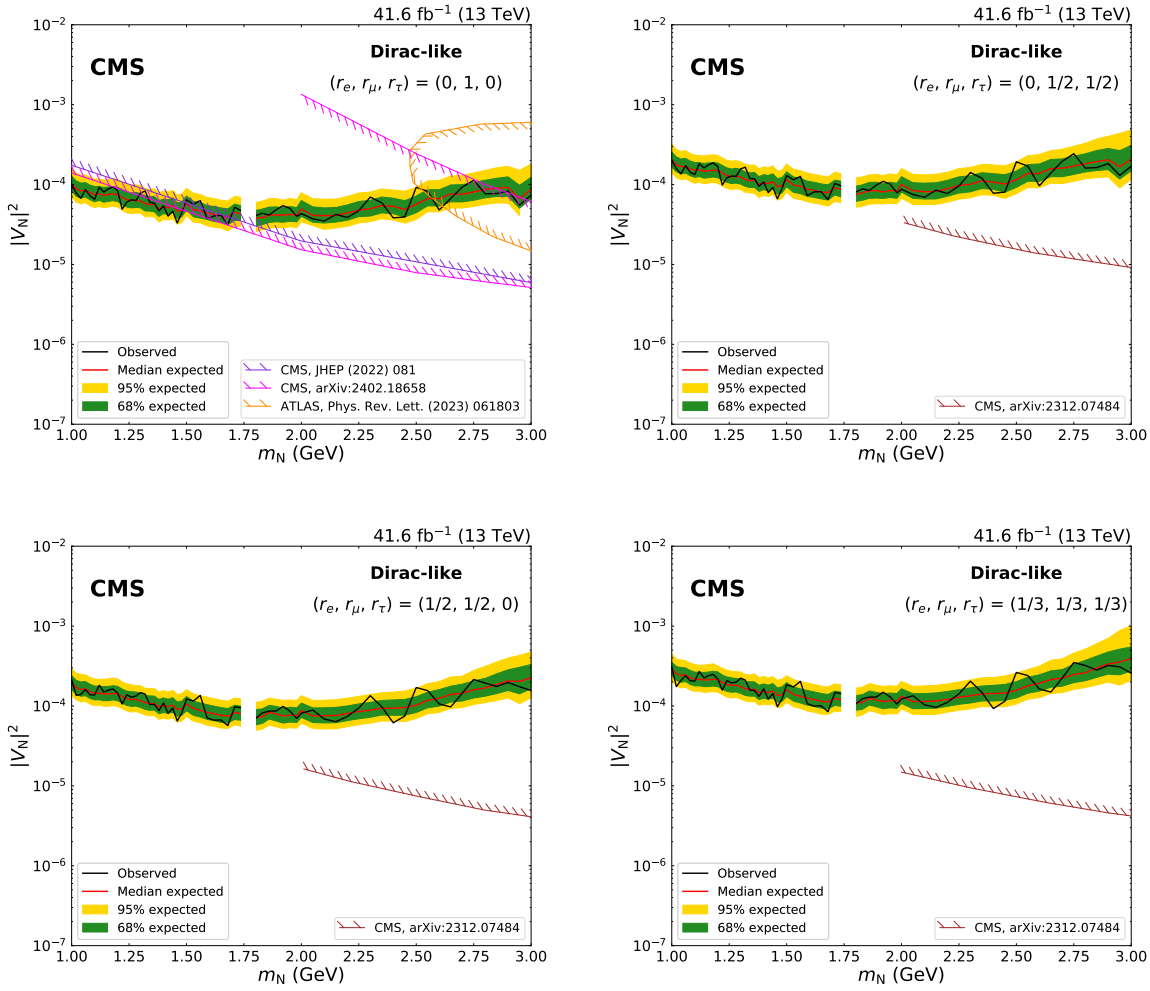

Figure 10: Expected and observed 95% CL limits on $|V_N|^2$ as a function of m_N, in the Dirac-like scenario. On the upper row, the limits are derived uniquely with the dimuon channel, and are shown for the mixing scenarios $(r_e, r_\mu, r_\tau) = (0, 1, 0)$ on the left and for $(r_e, r_\mu, r_\tau) = (0, 1/2, 1/2)$ on the right; on the lower row, the limits are obtained with the dimuon and mixed-flavour channel combined, for the mixing scenarios $(r_e, r_\mu, r_\tau) = (1/2, 1/2, 0)$ on the left and for $(r_e, r_\mu, r_\tau) = (1/3, 1/3, 1/3)$ on the right. In the upper left figure, results from the CMS [21, 23] and ATLAS [17] Collaborations are shown as a comparison; in the other figures, results from the CMS Collaboration [22] are reported. The mass range with no results shown corresponds to the D^0 meson veto listed in the lower part of Table 1.

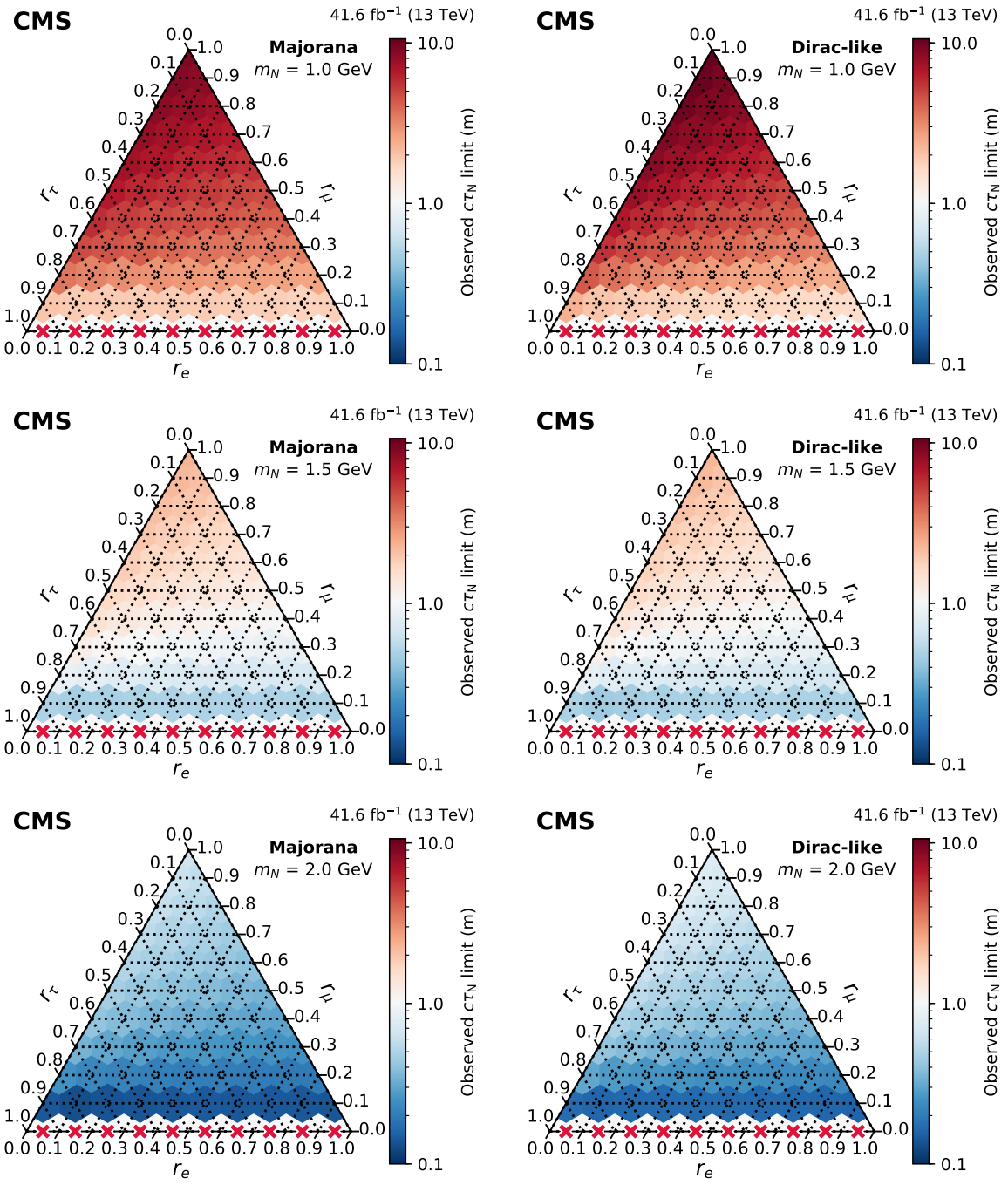

Figure 11: Observed 95% CL lower limits on $c\tau_{\mathrm{N}}$ as functions of the mixing ratios (r_{e}, r_μ, r_τ) for fixed N masses of 1 GeV (upper row), 1.5 GeV (middle row), and 2 GeV (lower row), in the Majorana (left column) and Dirac-like (right column) scenarios. The red crosses indicate that there is no exclusion found for that point. The orientation of the value markers on each axis identifies the associated internal lines on the plot.

Table 5: Summary of the most stringent lower limits on $c\tau_N$ at 95% CL, obtained for the mixing scenario $(r_e, r_\mu, r_\tau) = (0, 1, 0)$. The maximum excluded value of $c\tau_N$ is reported for masses m_N = 1.0, 1.5 and 2.0, and for the Majorana and Dirac-like scenarios.

Mass (GeV)	Scenario	$c\tau_N$ (m)
1.0	Majorana	9.2
1.5	Majorana	2.3
2.0	Majorana	0.7
1.0	Dirac-like	10.5
1.5	Dirac-like	2.2
2.0	Dirac-like	0.8

11 Summary

A search for long-lived heavy neutrinos, N, in the leptonic and semileptonic decays of B mesons produced in proton-proton collisions at $\sqrt{s} = 13\,\text{TeV}$ has been performed. The search uses a special data sample, referred to as the B-parking data sample, accumulated by the CMS experiment during 2018. The sample corresponds to an integrated luminosity of $41.6\,\text{fb}^{-1}$ and contains of order 10^{10} $\text{b}\bar{\text{b}}$ events.

The search is based on the process $\text{B} \to \ell_\text{B}\text{NX}$, $\text{N} \to \ell^\pm\pi^\mp$, where the charged leptons ℓ_B and ℓ are required to be $\ell_\text{B}\ell = \mu\mu$, μe, or $\text{e}\mu$; the hadronic recoil system, X, is treated inclusively and is not reconstructed and the $\text{B} = (\text{B}_\text{u}, \text{B}_\text{d}, \text{B}_\text{s}, \text{B}_\text{c})$ decays are summed. Results are reported for the N mass range $1 < m_N < 3\,\text{GeV}$.

The main elements of the search signature are (i) two charged leptons, at least one of which must be a muon that satisfies the B-parking trigger requirements, (ii) a displaced vertex associated with the $\text{N} \to \ell^\pm\pi^\mp$ decay, and (iii) a peak in the invariant mass distribution of the $\ell^\pm\pi^\mp$ system consistent with the expected signal shape. Backgrounds, which arise primarily from strong-interaction processes, are suppressed using a parametric neural network that considers a broad range of event properties.

A search for N states is performed using simultaneous maximum likelihood fits to the $\ell^\pm\pi^\mp$ invariant mass distributions in 24 mutually exclusive event categories. No significant excess of events over the SM background is observed in any of the fit regions.

The results are interpreted for the separate hypotheses of a Majorana or Dirac-like particle as (i) upper limits at 95% CL on $|V_N|^2$ as functions of m_N, for representative scenarios specified by different values of the mixing ratios r_e, r_μ, and r_τ; and as (ii) lower limits at 95% CL on $c\tau_N$ for 66 combinations of r_e, r_μ, and r_τ for signal masses $m_N = 1.0$, 1.5, and $2.0\,\text{GeV}$. The most stringent limits are $|V_N|^2 < 2.0 \times 10^{-5}$ and $c\tau_N > 10.5\,\text{m}$, obtained for the Majorana and Dirac-like cases, respectively, and for the scenario in which the N mixes exclusively with the muon sector.

This search provides the most stringent exclusion limits on $|V_N|^2$ for masses $1 < m_N < 1.7\,\text{GeV}$ from a collider experiment to date. Assuming the benchmark scenario $(r_e, r_\mu, r_\tau) = (0, 1, 0)$ and the Majorana hypothesis, the exclusion is improved by almost one order of magnitude compared to LHCb [24], and by up to a factor of about 2 compared to Belle [14] and the most stringent previous hadron collider result [23]. Furthermore, the first upper limits on $|V_N|^2$ are set for the mass range $1 < m_N < 2\,\text{GeV}$ for the mixing scenarios $(r_e, r_\mu, r_\tau) = (0, 1/2, 1/2)$, $(1/2, 1/2, 0)$, and $(1/3, 1/3, 1/3)$. Finally, lower limits on $c\tau_N$ in the form of

ternary plots for masses $m_{\mathrm{N}} \leq 2.0\,\mathrm{GeV}$ are presented for the first time.

Acknowledgments

We congratulate our colleagues in the CERN accelerator departments for the excellent performance of the LHC and thank the technical and administrative staffs at CERN and at other CMS institutes for their contributions to the success of the CMS effort. In addition, we gratefully acknowledge the computing centres and personnel of the Worldwide LHC Computing Grid and other centres for delivering so effectively the computing infrastructure essential to our analyses. Finally, we acknowledge the enduring support for the construction and operation of the LHC, the CMS detector, and the supporting computing infrastructure provided by the following funding agencies: SC (Armenia), BMBWF and FWF (Austria); FNRS and FWO (Belgium); CNPq, CAPES, FAPERJ, FAPERGS, and FAPESP (Brazil); MES and BNSF (Bulgaria); CERN; CAS, MoST, and NSFC (China); MINCIENCIAS (Colombia); MSES and CSF (Croatia); RIF (Cyprus); SENESCYT (Ecuador); ERC PRG, RVTT3 and MoER TK202 (Estonia); Academy of Finland, MEC, and HIP (Finland); CEA and CNRS/IN2P3 (France); SRNSF (Georgia); BMBF, DFG, and HGF (Germany); GSRI (Greece); NKFIH (Hungary); DAE and DST (India); IPM (Iran); SFI (Ireland); INFN (Italy); MSIP and NRF (Republic of Korea); MES (Latvia); LMTLT (Lithuania); MOE and UM (Malaysia); BUAP, CINVESTAV, CONACYT, LNS, SEP, and UASLP-FAI (Mexico); MOS (Montenegro); MBIE (New Zealand); PAEC (Pakistan); MES and NSC (Poland); FCT (Portugal); MESTD (Serbia); MCIN/AEI and PCTI (Spain); MOSTR (Sri Lanka); Swiss Funding Agencies (Switzerland); MST (Taipei); MHESI and NSTDA (Thailand); TUBITAK and TENMAK (Turkey); NASU (Ukraine); STFC (United Kingdom); DOE and NSF (USA).

Individuals have received support from the Marie-Curie programme and the European Research Council and Horizon 2020 Grant, contract Nos. 675440, 724704, 752730, 758316, 765710, 824093, 101115353, and COST Action CA16108 (European Union); the Leventis Foundation; the Alfred P. Sloan Foundation; the Alexander von Humboldt Foundation; the Science Committee, project no. 22rl-037 (Armenia); the Belgian Federal Science Policy Office; the Fonds pour la Formation à la Recherche dans l'Industrie et dans l'Agriculture (FRIA-Belgium); the Agentschap voor Innovatie door Wetenschap en Technologie (IWT-Belgium); the F.R.S.-FNRS and FWO (Belgium) under the "Excellence of Science – EOS" – be.h project n. 30820817; the Beijing Municipal Science & Technology Commission, No. Z191100007219010 and Fundamental Research Funds for the Central Universities (China); the Ministry of Education, Youth and Sports (MEYS) of the Czech Republic; the Shota Rustaveli National Science Foundation, grant FR-22-985 (Georgia); the Deutsche Forschungsgemeinschaft (DFG), under Germany's Excellence Strategy – EXC 2121 "Quantum Universe" – 390833306, and under project number 400140256 - GRK2497; the Hellenic Foundation for Research and Innovation (HFRI), Project Number 2288 (Greece); the Hungarian Academy of Sciences, the New National Excellence Program - ÚNKP, the NKFIH research grants K 124845, K 124850, K 128713, K 128786, K 129058, K 131991, K 133046, K 138136, K 143460, K 143477, 2020-2.2.1-ED-2021-00181, and TKP2021-NKTA-64 (Hungary); the Council of Science and Industrial Research, India; ICSC – National Research Centre for High Performance Computing, Big Data and Quantum Computing, funded by the EU NexGeneration program (Italy); the Latvian Council of Science; the Ministry of Education and Science, project no. 2022/WK/14, and the National Science Center, contracts Opus 2021/41/B/ST2/01369 and 2021/43/B/ST2/01552 (Poland); the Fundação para a Ciência e a Tecnologia, grant CEECIND/01334/2018 (Portugal); the National Priorities Research Program by Qatar National Research Fund; MCIN/AEI/10.13039/501100011033, ERDF "a way of making Europe", and the Programa Estatal de Fomento de la Investigación Científica y Técnica de

Excelencia María de Maeztu, grant MDM-2017-0765 and Programa Severo Ochoa del Principado de Asturias (Spain); the Chulalongkorn Academic into Its 2nd Century Project Advancement Project, and the National Science, Research and Innovation Fund via the Program Management Unit for Human Resources & Institutional Development, Research and Innovation, grant B37G660013 (Thailand); the Kavli Foundation; the Nvidia Corporation; the SuperMicro Corporation; the Welch Foundation, contract C-1845; and the Weston Havens Foundation (USA).

References

[1] S. Bilenky, "Neutrino oscillations: From a historical perspective to the present status", *Nucl. Phys. B* **908** (2016) 2, doi:10.1016/j.nuclphysb.2016.01.025, arXiv:1602.00170.

[2] J. Silk et al., "Particle dark matter: observations, models and searches". Cambridge Univ. Press, Cambridge, 2010. doi:10.1017/CBO9780511770739, ISBN 978-1-107-65392-4.

[3] G. R. Farrar and M. E. Shaposhnikov, "Baryon asymmetry of the universe in the standard electroweak theory", *Phys. Rev. D* **50** (1994) 774, doi:10.1103/PhysRevD.50.774, arXiv:hep-ph/9305275.

[4] T. Asaka, S. Blanchet, and M. Shaposhnikov, "The nuMSM, dark matter and neutrino masses", *Phys. Lett. B* **631** (2005) 151, doi:10.1016/j.physletb.2005.09.070, arXiv:hep-ph/0503065.

[5] T. Asaka and M. Shaposhnikov, "The νMSM, dark matter and baryon asymmetry of the universe", *Phys. Lett. B* **620** (2005) 17, doi:10.1016/j.physletb.2005.06.020, arXiv:hep-ph/0505013.

[6] S. Dodelson and L. M. Widrow, "Sterile-neutrinos as dark matter", *Phys. Rev. Lett.* **72** (1994) 17, doi:10.1103/PhysRevLett.72.17, arXiv:hep-ph/9303287.

[7] M. Fukugita and T. Yanagida, "Baryogenesis without grand unification", *Phys. Lett. B* **174** (1986) 45, doi:10.1016/0370-2693(86)91126-3.

[8] P. Minkowski, "$\mu \to e\gamma$ at a rate of one out of 10^9 muon decays?", *Phys. Lett. B* **67** (1977) 421, doi:10.1016/0370-2693(77)90435-X.

[9] K. Bondarenko, A. Boyarsky, D. Gorbunov, and O. Ruchayskiy, "Phenomenology of GeV-scale heavy neutral leptons", *JHEP* **11** (2018) 032, doi:10.1007/JHEP11(2018)032, arXiv:1805.08567.

[10] CHARM Collaboration, "A search for decays of heavy neutrinos in the mass range 0.5 - 2.8 GeV", *Phys. Lett. B* **166** (1986) 473, doi:10.1016/0370-2693(86)91601-1.

[11] NuTeV-E815 Collaboration, "Search for neutral heavy leptons in a high-energy neutrino beam", *Phys. Rev. Lett.* **83** (1999) 4943, doi:10.1103/PhysRevLett.83.4943, arXiv:hep-ex/9908011.

[12] R. Barouki, G. Marocco, and S. Sarkar, "Blast from the past II: Constraints on heavy neutral leptons from the BEBC WA66 beam dump experiment", *SciPost Phys.* **13** (2022) 118, doi:10.21468/SciPostPhys.13.5.118, arXiv:2208.00416.

[13] WA66 Collaboration, "Search for heavy neutrino decays in the BEBC beam dump experiment", *Phys. Lett. B* **160** (1985) 207, doi:10.1016/0370-2693(85)91493-5.

[14] Belle Collaboration, "Search for heavy neutrinos at Belle", *Phys. Rev. D* **87** (2013) 071102, doi:10.1103/PhysRevD.87.071102, arXiv:1301.1105. [Erratum: Phys. Rev. D 95 (2017) 099903].

[15] BABAR Collaboration, "Search for heavy neutral leptons using tau lepton decays at BABAR", *Phys. Rev. D* **107** (2023) 052009, doi:10.1103/PhysRevD.107.052009, arXiv:2207.09575.

[16] ATLAS Collaboration, "Search for heavy neutral leptons in decays of *W* bosons produced in 13 TeV *pp* collisions using prompt and displaced signatures with the ATLAS detector", *JHEP* **10** (2019) 265, doi:10.1007/JHEP10(2019)265, arXiv:1905.09787.

[17] ATLAS Collaboration, "Search for heavy neutral leptons in decays of W bosons using a dilepton displaced vertex in $\sqrt{s} = 13$ TeV pp collisions with the ATLAS detector", *Phys. Rev. Lett.* **131** (2023) 061803, doi:10.1103/PhysRevLett.131.061803, arXiv:2204.11988.

[18] CMS Collaboration, "Search for heavy neutral leptons in events with three charged leptons in proton-proton collisions at $\sqrt{s} = 13$ TeV", *Phys. Rev. Lett.* **120** (2018) 221801, doi:10.1103/PhysRevLett.120.221801, arXiv:1802.02965.

[19] CMS Collaboration, "Search for heavy Majorana neutrinos in same-sign dilepton channels in proton-proton collisions at $\sqrt{s} = 13$ TeV", *JHEP* **01** (2019) 122, doi:10.1007/JHEP01(2019)122, arXiv:1806.10905.

[20] CMS Collaboration, "Search for heavy neutrinos and third-generation leptoquarks in hadronic states of two τ leptons and two jets in proton-proton collisions at $\sqrt{s} = 13$ TeV", *JHEP* **03** (2019) 170, doi:10.1007/JHEP03(2019)170, arXiv:1811.00806.

[21] CMS Collaboration, "Search for long-lived heavy neutral leptons with displaced vertices in proton-proton collisions at $\sqrt{s}$ =13 TeV", *JHEP* **07** (2022) 081, doi:10.1007/JHEP07(2022)081, arXiv:2201.05578.

[22] CMS Collaboration, "Search for long-lived heavy neutral leptons with lepton flavour conserving or violating decays to a jet and a charged lepton", 2023. arXiv:2312.07484.

[23] CMS Collaboration, "Search for long-lived heavy neutral leptons decaying in the CMS muon detectors in proton-proton collisions at $\sqrt{s}$ = 13 TeV", 2, 2024. arXiv:2402.18658.

[24] LHCb Collaboration, "Search for Majorana neutrinos in $B^- \to \pi^+\mu^-\mu^-$ decays", *Phys. Rev. Lett.* **112** (2014) 131802, doi:10.1103/PhysRevLett.112.131802, arXiv:1401.5361.

[25] LHCb Collaboration, "Search for heavy neutral leptons in $W^+ \to \mu^+\mu^\pm$jet decays", *Eur. Phys. J. C* **81** (2021) 248, doi:10.1140/epjc/s10052-021-08973-5, arXiv:2011.05263.

[26] CMS Collaboration, "Test of lepton flavor universality in $B^\pm \to K^\pm\mu^+\mu^-$ and $B^\pm \to K^\pm e^+e^-$ decays in proton-proton collisions at $\sqrt{s}$ = 13 TeV", 2024. arXiv:2401.07090.

[27] F. F. Deppisch, P. S. Bhupal Dev, and A. Pilaftsis, "Neutrinos and Collider Physics", *New J. Phys.* **17** (2015) 075019, doi:10.1088/1367-2630/17/7/075019, arXiv:1502.06541.

[28] Particle Data Group, "Review of particle physics", *PTEP* **2022** (2022) 083C01, doi:10.1093/ptep/ptac097.

[29] M. Drewes, "The phenomenology of right handed neutrinos", *Int. J. Mod. Phys. E* **22** (2013) 1330019, doi:10.1142/S0218301313300191, arXiv:1303.6912.

[30] P. Hernández, J. Jones-Pérez, and O. Suarez-Navarro, "Majorana vs pseudo-Dirac neutrinos at the ILC", *Eur. Phys. J. C* **79** (2019) 220, doi:10.1140/epjc/s10052-019-6728-1, arXiv:1810.07210.

[31] HEPData record for this analysis, 2024. doi:10.17182/hepdata.147308.

[32] CMS Collaboration, "Performance of the CMS Level-1 trigger in proton-proton collisions at $\sqrt{s} = 13\,\text{TeV}$", *JINST* **15** (2020) P10017, doi:10.1088/1748-0221/15/10/P10017, arXiv:2006.10165.

[33] CMS Collaboration, "The CMS trigger system", *JINST* **12** (2017) P01020, doi:10.1088/1748-0221/12/01/P01020, arXiv:1609.02366.

[34] CMS Collaboration, "The CMS experiment at the CERN LHC", *JINST* **3** (2008) S08004, doi:10.1088/1748-0221/3/08/S08004.

[35] CMS Collaboration, "CMS luminosity measurement for the 2018 data-taking period at $\sqrt{s} = 13\,\text{TeV}$", CMS Physics Analysis Summary CMS-PAS-LUM-18-002, 2019.

[36] LHCb Collaboration, "Measurement of the B_c^- meson production fraction and asymmetry in 7 and 13 TeV pp collisions", *Phys. Rev. D* **100** (2019) 112006, doi:10.1103/PhysRevD.100.112006, arXiv:1910.13404.

[37] T. Sjöstrand et al., "An introduction to PYTHIA 8.2", *Comput. Phys. Commun.* **191** (2015) 159, doi:10.1016/j.cpc.2015.01.024, arXiv:1410.3012.

[38] CMS Collaboration, "Extraction and validation of a new set of CMS PYTHIA8 tunes from underlying-event measurements", *Eur. Phys. J. C* **80** (2020) 4, doi:10.1140/epjc/s10052-019-7499-4, arXiv:1903.12179.

[39] NNPDF Collaboration, "Parton distributions from high-precision collider data", *Eur. Phys. J. C* **77** (2017) 663, doi:10.1140/epjc/s10052-017-5199-5, arXiv:1706.00428.

[40] D. J. Lange, "The EvtGen particle decay simulation package", *Nucl. Instrum. Meth. A* **462** (2001) 152, doi:10.1016/S0168-9002(01)00089-4.

[41] C.-H. Chang, J.-X. Wang, and X.-G. Wu, "BCVEGPY2.0: A Upgrade version of the generator BCVEGPY with an addendum about hadroproduction of the P-wave B(c) states", *Comput. Phys. Commun.* **174** (2006) 241, doi:10.1016/j.cpc.2005.09.008, arXiv:hep-ph/0504017.

[42] GEANT4 Collaboration, "GEANT4—a simulation toolkit", *Nucl. Instrum. Meth. A* **506** (2003) 250, doi:10.1016/S0168-9002(03)01368-8.

[43] CMS Collaboration, "Performance of the CMS muon detector and muon reconstruction with proton-proton collisions at $\sqrt{s} = 13$ TeV", *JINST* **13** (2018) P06015, doi:10.1088/1748-0221/13/06/P06015, arXiv:1804.04528.

[44] CMS Collaboration, "Particle-flow reconstruction and global event description with the CMS detector", *JINST* **12** (2017) P10003, doi:10.1088/1748-0221/12/10/P10003, arXiv:1706.04965.

[45] CMS Collaboration, "CMS tracking performance results from early LHC operation", *Eur. Phys. J. C* **70** (2010) 1165, doi:10.1140/epjc/s10052-010-1491-3, arXiv:1007.1988.

[46] CMS Collaboration, "Electron and photon reconstruction and identification with the CMS experiment at the CERN LHC", *JINST* **16** (2021) P05014, doi:10.1088/1748-0221/16/05/P05014, arXiv:2012.06888.

[47] K. Prokofiev and T. Speer, "A kinematic and a decay chain reconstruction library", in *14th International Conference on Computing in High-Energy and Nuclear Physics*, p. 411. 2005.

[48] P. Baldi et al., "Parameterized neural networks for high-energy physics", *Eur. Phys. J. C* **76** (2016) 235, doi:10.1140/epjc/s10052-016-4099-4, arXiv:1601.07913.

[49] K. Fukushima, "Visual feature extraction by a multilayered network of analog threshold elements", *IEEE Transactions on Systems Science and Cybernetics* **5** (1969) 322, doi:10.1109/TSSC.1969.300225.

[50] F. Chollet et al., "Keras". https://keras.io, 2015.

[51] M. Abadi et al., "TensorFlow: A system for large-scale machine learning", in *Proceedings of the 12th USENIX Conference on Operating Systems Design and Implementation*, OSDI'16, p. 265. USENIX Association, USA, 2016. arXiv:1605.08695.

[52] D. P. Kingma and J. Ba, "Adam: A method for stochastic optimization", 2014. arXiv:1412.6980.

[53] F. Pedregosa et al., "Scikit-learn: Machine learning in Python", *J. Mach. Learn. Res.* **12** (2011) 2825, arXiv:1201.0490.

[54] CMS Collaboration, "Measurement of the total and differential inclusive B^+ hadron cross sections in pp collisions at $\sqrt{s}$ = 13 TeV", *Phys. Lett. B* **771** (2017) 435, doi:10.1016/j.physletb.2017.05.074, arXiv:1609.00873.

[55] M. J. Oreglia, "A study of the reactions $\psi' \to \gamma\gamma\psi$". PhD thesis, Stanford University, 1980. SLAC Report SLAC-R-236.

[56] J. E. Gaiser, "Charmonium spectroscopy from radiative decays of the J/ψ and ψ'". PhD thesis, Stanford University, 1982. SLAC Report SLAC-R-255.

[57] P. D. Dauncey, M. Kenzie, N. Wardle, and G. J. Davies, "Handling uncertainties in background shapes: the discrete profiling method", *JINST* **10** (2015) P04015, doi:10.1088/1748-0221/10/04/P04015, arXiv:1408.6865.

[58] R. A. Fisher, "On the mathematical foundations of theoretical statistics", *Phil. Trans. Roy. Soc. Lond. A* **222** (1922) 309, doi:10.1098/rsta.1922.0009.

[59] S. S. Wilks, "The large-sample distribution of the likelihood ratio for testing composite hypotheses", *Annals Math. Statist.* **9** (1938) 60, doi:10.1214/aoms/1177732360.

[60] A. L. Read, "Presentation of search results: The CL_s technique", *J. Phys. G* **28** (2002) 2693, doi:10.1088/0954-3899/28/10/313.

[61] G. Cowan, K. Cranmer, E. Gross, and O. Vitells, "Asymptotic formulae for likelihood-based tests of new physics", *Eur. Phys. J. C* **71** (2011) 1554, doi:10.1140/epjc/s10052-011-1554-0, arXiv:1007.1727. [Erratum: Eur. Phys. J. C 73 (2013) 2501].

[62] M. Drewes, J. Klarić, and J. López-Pavón, "New benchmark models for heavy neutral lepton searches", *Eur. Phys. J. C* **82** (2022) 1176, doi:10.1140/epjc/s10052-022-11100-7, arXiv:2207.02742.

[63] B. Shuve and M. E. Peskin, "Revision of the LHCb limit on Majorana neutrinos", *Phys. Rev. D* **94** (2016) 113007, doi:10.1103/PhysRevD.94.113007, arXiv:1607.04258.

A The CMS Collaboration

Yerevan Physics Institute, Yerevan, Armenia
A. Hayrapetyan, A. Tumasyan[1]

Institut für Hochenergiephysik, Vienna, Austria
W. Adam, J.W. Andrejkovic, T. Bergauer, S. Chatterjee, K. Damanakis, M. Dragicevic, P.S. Hussain, M. Jeitler[2], N. Krammer, A. Li, D. Liko, I. Mikulec, J. Schieck[2], R. Schöfbeck, D. Schwarz, M. Sonawane, S. Templ, W. Waltenberger, C.-E. Wulz[2]

Universiteit Antwerpen, Antwerpen, Belgium
M.R. Darwish[3], T. Janssen, P. Van Mechelen

Vrije Universiteit Brussel, Brussel, Belgium
N. Breugelmans, J. D'Hondt, S. Dansana, A. De Moor, M. Delcourt, F. Heyen, S. Lowette, I. Makarenko, D. Müller, S. Tavernier, M. Tytgat[4], G.P. Van Onsem, S. Van Putte, D. Vannerom

Université Libre de Bruxelles, Bruxelles, Belgium
B. Clerbaux, A.K. Das, G. De Lentdecker, H. Evard, L. Favart, P. Gianneios, D. Hohov, J. Jaramillo, A. Khalilzadeh, F.A. Khan, K. Lee, M. Mahdavikhorrami, A. Malara, S. Paredes, L. Thomas, M. Vanden Bemden, C. Vander Velde, P. Vanlaer

Ghent University, Ghent, Belgium
M. De Coen, D. Dobur, G. Gokbulut, Y. Hong, J. Knolle, L. Lambrecht, D. Marckx, G. Mestdach, K. Mota Amarilo, C. Rendón, A. Samalan, K. Skovpen, N. Van Den Bossche, J. van der Linden, L. Wezenbeek

Université Catholique de Louvain, Louvain-la-Neuve, Belgium
A. Benecke, A. Bethani, G. Bruno, C. Caputo, J. De Favereau De Jeneret, C. Delaere, I.S. Donertas, A. Giammanco, A.O. Guzel, Sa. Jain, V. Lemaitre, J. Lidrych, P. Mastrapasqua, T.T. Tran, S. Wertz

Centro Brasileiro de Pesquisas Fisicas, Rio de Janeiro, Brazil
G.A. Alves, E. Coelho, C. Hensel, T. Menezes De Oliveira, A. Moraes, P. Rebello Teles, M. Soeiro, A. Vilela Pereira[5]

Universidade do Estado do Rio de Janeiro, Rio de Janeiro, Brazil
W.L. Aldá Júnior, M. Alves Gallo Pereira, M. Barroso Ferreira Filho, H. Brandao Malbouisson, W. Carvalho, J. Chinellato[6], E.M. Da Costa, G.G. Da Silveira[7], D. De Jesus Damiao, S. Fonseca De Souza, R. Gomes De Souza, M. Macedo, J. Martins[8], C. Mora Herrera, L. Mundim, H. Nogima, J.P. Pinheiro, A. Santoro, A. Sznajder, M. Thiel

Universidade Estadual Paulista, Universidade Federal do ABC, São Paulo, Brazil
C.A. Bernardes[7], L. Calligaris, T.R. Fernandez Perez Tomei, E.M. Gregores, I. Maietto Silverio, P.G. Mercadante, S.F. Novaes, B. Orzari, Sandra S. Padula

Institute for Nuclear Research and Nuclear Energy, Bulgarian Academy of Sciences, Sofia, Bulgaria
A. Aleksandrov, G. Antchev, R. Hadjiiska, P. Iaydjiev, M. Misheva, M. Shopova, G. Sultanov

University of Sofia, Sofia, Bulgaria
A. Dimitrov, L. Litov, B. Pavlov, P. Petkov, A. Petrov, E. Shumka

Instituto De Alta Investigación, Universidad de Tarapacá, Casilla 7 D, Arica, Chile
S. Keshri, S. Thakur

Beihang University, Beijing, China
T. Cheng, T. Javaid, L. Yuan

Department of Physics, Tsinghua University, Beijing, China
Z. Hu, Z. Liang, J. Liu, K. Yi[9,10]

Institute of High Energy Physics, Beijing, China
G.M. Chen[11], H.S. Chen[11], M. Chen[11], F. Iemmi, C.H. Jiang, A. Kapoor[12], H. Liao, Z.-A. Liu[13], R. Sharma[14], J.N. Song[13], J. Tao, C. Wang[11], J. Wang, Z. Wang[11], H. Zhang, J. Zhao

State Key Laboratory of Nuclear Physics and Technology, Peking University, Beijing, China
A. Agapitos, Y. Ban, S. Deng, B. Guo, A. Levin, C. Li, Q. Li, Y. Mao, S. Qian, S.J. Qian, X. Sun, D. Wang, H. Yang, L. Zhang, Y. Zhao, C. Zhou

Guangdong Provincial Key Laboratory of Nuclear Science and Guangdong-Hong Kong Joint Laboratory of Quantum Matter, South China Normal University, Guangzhou, China
S. Yang

Sun Yat-Sen University, Guangzhou, China
Z. You

University of Science and Technology of China, Hefei, China
K. Jaffel, N. Lu

Nanjing Normal University, Nanjing, China
G. Bauer[15], B. Li, J. Zhang

Institute of Modern Physics and Key Laboratory of Nuclear Physics and Ion-beam Application (MOE) - Fudan University, Shanghai, China
X. Gao[16]

Zhejiang University, Hangzhou, Zhejiang, China
Z. Lin, C. Lu, M. Xiao

Universidad de Los Andes, Bogota, Colombia
C. Avila, D.A. Barbosa Trujillo, A. Cabrera, C. Florez, J. Fraga, J.A. Reyes Vega

Universidad de Antioquia, Medellin, Colombia
F. Ramirez, M. Rodriguez, A.A. Ruales Barbosa, J.D. Ruiz Alvarez

University of Split, Faculty of Electrical Engineering, Mechanical Engineering and Naval Architecture, Split, Croatia
D. Giljanovic, N. Godinovic, D. Lelas, A. Sculac

University of Split, Faculty of Science, Split, Croatia
M. Kovac, A. Petkovic, T. Sculac

Institute Rudjer Boskovic, Zagreb, Croatia
P. Bargassa, V. Brigljevic, B.K. Chitroda, D. Ferencek, K. Jakovcic, S. Mishra, A. Starodumov[17], T. Susa

University of Cyprus, Nicosia, Cyprus
A. Attikis, K. Christoforou, A. Hadjiagapiou, C. Leonidou, J. Mousa, C. Nicolaou, L. Paizanos, F. Ptochos, P.A. Razis, H. Rykaczewski, H. Saka, A. Stepennov

Charles University, Prague, Czech Republic
M. Finger, M. Finger Jr., A. Kveton

Universidad San Francisco de Quito, Quito, Ecuador
E. Carrera Jarrin

Academy of Scientific Research and Technology of the Arab Republic of Egypt, Egyptian Network of High Energy Physics, Cairo, Egypt
Y. Assran[18,19], S. Elgammal[19]

Center for High Energy Physics (CHEP-FU), Fayoum University, El-Fayoum, Egypt
M.A. Mahmoud, Y. Mohammed

National Institute of Chemical Physics and Biophysics, Tallinn, Estonia
K. Ehataht, M. Kadastik, T. Lange, S. Nandan, C. Nielsen, J. Pata, M. Raidal, L. Tani

Department of Physics, University of Helsinki, Helsinki, Finland
H. Kirschenmann, K. Osterberg, M. Voutilainen

Helsinki Institute of Physics, Helsinki, Finland
S. Bharthuar, E. Brücken, F. Garcia, P. Inkaew, K.T.S. Kallonen, R. Kinnunen, T. Lampén, K. Lassila-Perini, S. Lehti, T. Lindén, L. Martikainen, M. Myllymäki, M.m. Rantanen, H. Siikonen, J. Tuominiemi

Lappeenranta-Lahti University of Technology, Lappeenranta, Finland
P. Luukka, H. Petrow

IRFU, CEA, Université Paris-Saclay, Gif-sur-Yvette, France
M. Besancon, F. Couderc, M. Dejardin, D. Denegri, J.L. Faure, F. Ferri, S. Ganjour, P. Gras, G. Hamel de Monchenault, V. Lohezic, J. Malcles, F. Orlandi, L. Portales, J. Rander, A. Rosowsky, M.Ö. Sahin, A. Savoy-Navarro[20], P. Simkina, M. Titov, M. Tornago

Laboratoire Leprince-Ringuet, CNRS/IN2P3, Ecole Polytechnique, Institut Polytechnique de Paris, Palaiseau, France
F. Beaudette, P. Busson, A. Cappati, C. Charlot, M. Chiusi, F. Damas, O. Davignon, A. De Wit, I.T. Ehle, B.A. Fontana Santos Alves, S. Ghosh, A. Gilbert, R. Granier de Cassagnac, A. Hakimi, B. Harikrishnan, L. Kalipoliti, G. Liu, M. Nguyen, C. Ochando, R. Salerno, J.B. Sauvan, Y. Sirois, A. Tarabini, E. Vernazza, A. Zabi, A. Zghiche

Université de Strasbourg, CNRS, IPHC UMR 7178, Strasbourg, France
J.-L. Agram[21], J. Andrea, D. Apparu, D. Bloch, J.-M. Brom, E.C. Chabert, C. Collard, S. Falke, U. Goerlach, R. Haeberle, A.-C. Le Bihan, M. Meena, O. Poncet, G. Saha, M.A. Sessini, P. Van Hove, P. Vaucelle

Institut de Physique des 2 Infinis de Lyon (IP2I), Villeurbanne, France
D. Amram, S. Beauceron, B. Blancon, G. Boudoul, N. Chanon, D. Contardo, P. Depasse, C. Dozen[22], H. El Mamouni, J. Fay, S. Gascon, M. Gouzevitch, C. Greenberg, G. Grenier, B. Ille, E. Jourd'huy, I.B. Laktineh, M. Lethuillier, L. Mirabito,

S. Perries, A. Purohit, M. Vander Donckt, P. Verdier, J. Xiao

Georgian Technical University, Tbilisi, Georgia
A. Khvedelidze[17], I. Lomidze, Z. Tsamalaidze[17]

RWTH Aachen University, I. Physikalisches Institut, Aachen, Germany
V. Botta, L. Feld, K. Klein, M. Lipinski, D. Meuser, A. Pauls, N. Röwert, M. Teroerde

RWTH Aachen University, III. Physikalisches Institut A, Aachen, Germany
S. Diekmann, A. Dodonova, N. Eich, D. Eliseev, F. Engelke, J. Erdmann, M. Erdmann, P. Fackeldey, B. Fischer, T. Hebbeker, K. Hoepfner, F. Ivone, A. Jung, M.y. Lee, F. Mausolf, M. Merschmeyer, A. Meyer, S. Mukherjee, D. Noll, F. Nowotny, A. Pozdnyakov, Y. Rath, W. Redjeb, F. Rehm, H. Reithler, V. Sarkisovi, A. Schmidt, A. Sharma, J.L. Spah, A. Stein, F. Torres Da Silva De Araujo[23], S. Wiedenbeck, S. Zaleski

RWTH Aachen University, III. Physikalisches Institut B, Aachen, Germany
C. Dziwok, G. Flügge, T. Kress, A. Nowack, O. Pooth, A. Stahl, T. Ziemons, A. Zotz

Deutsches Elektronen-Synchrotron, Hamburg, Germany
H. Aarup Petersen, M. Aldaya Martin, J. Alimena, S. Amoroso, J. Bach, S. Baxter, M. Bayatmakou, H. Becerril Gonzalez, O. Behnke, A. Belvedere, S. Bhattacharya, F. Blekman[24], K. Borras[25], A. Campbell, A. Cardini, C. Cheng, F. Colombina, S. Consuegra Rodríguez, G. Correia Silva, M. De Silva, G. Eckerlin, D. Eckstein, L.I. Estevez Banos, O. Filatov, E. Gallo[24], A. Geiser, V. Guglielmi, M. Guthoff, A. Hinzmann, L. Jeppe, B. Kaech, M. Kasemann, C. Kleinwort, R. Kogler, M. Komm, D. Krücker, W. Lange, D. Leyva Pernia, K. Lipka[26], W. Lohmann[27], R. Mankel, I.-A. Melzer-Pellmann, A.B. Meyer, G. Milella, K. Moral Figueroa, A. Mussgiller, L.P. Nair, J. Niedziela, A. Nürnberg, Y. Otarid, D. Pérez Adán, E. Ranken, A. Raspereza, D. Rastorguev, J. Rübenach, L. Rygaard, A. Saggio, M. Scham[28,25], S. Schnake[25], P. Schütze, C. Schwanenberger[24], D. Selivanova, K. Sharko, M. Shchedrolosiev, D. Stafford, F. Vazzoler, A. Ventura Barroso, R. Walsh, D. Wang, Q. Wang, Y. Wen, K. Wichmann, L. Wiens[25], C. Wissing, Y. Yang, A. Zimermmane Castro Santos

University of Hamburg, Hamburg, Germany
A. Albrecht, S. Albrecht, M. Antonello, S. Bein, L. Benato, S. Bollweg, M. Bonanomi, P. Connor, K. El Morabit, Y. Fischer, E. Garutti, A. Grohsjean, J. Haller, H.R. Jabusch, G. Kasieczka, P. Keicher, R. Klanner, W. Korcari, T. Kramer, C.c. Kuo, V. Kutzner, F. Labe, J. Lange, A. Lobanov, C. Matthies, L. Moureaux, M. Mrowietz, A. Nigamova, Y. Nissan, A. Paasch, K.J. Pena Rodriguez, T. Quadfasel, B. Raciti, M. Rieger, D. Savoiu, J. Schindler, P. Schleper, M. Schröder, J. Schwandt, M. Sommerhalder, H. Stadie, G. Steinbrück, A. Tews, M. Wolf

Karlsruher Institut fuer Technologie, Karlsruhe, Germany
S. Brommer, M. Burkart, E. Butz, T. Chwalek, A. Dierlamm, A. Droll, N. Faltermann, M. Giffels, A. Gottmann, F. Hartmann[29], R. Hofsaess, M. Horzela, U. Husemann, J. Kieseler, M. Klute, R. Koppenhöfer, J.M. Lawhorn, M. Link, A. Lintuluoto, B. Maier, S. Maier, S. Mitra, M. Mormile, Th. Müller, M. Neukum, M. Oh, E. Pfeffer, M. Presilla, G. Quast, K. Rabbertz, B. Regnery, N. Shadskiy,

I. Shvetsov, H.J. Simonis, L. Sowa, L. Stockmeier, K. Tauqeer, M. Toms, N. Trevisani, R.F. Von Cube, M. Wassmer, S. Wieland, F. Wittig, R. Wolf, X. Zuo

Institute of Nuclear and Particle Physics (INPP), NCSR Demokritos, Aghia Paraskevi, Greece
G. Anagnostou, G. Daskalakis, A. Kyriakis, A. Papadopoulos[29], A. Stakia

National and Kapodistrian University of Athens, Athens, Greece
P. Kontaxakis, G. Melachroinos, Z. Painesis, A. Panagiotou, I. Papavergou, I. Paraskevas, N. Saoulidou, K. Theofilatos, E. Tziaferi, K. Vellidis, I. Zisopoulos

National Technical University of Athens, Athens, Greece
G. Bakas, T. Chatzistavrou, G. Karapostoli, K. Kousouris, I. Papakrivopoulos, E. Siamarkou, G. Tsipolitis, A. Zacharopoulou

University of Ioánnina, Ioánnina, Greece
K. Adamidis, I. Bestintzanos, I. Evangelou, C. Foudas, C. Kamtsikis, P. Katsoulis, P. Kokkas, P.G. Kosmoglou Kioseoglou, N. Manthos, I. Papadopoulos, J. Strologas

HUN-REN Wigner Research Centre for Physics, Budapest, Hungary
M. Bartók[30], C. Hajdu, D. Horvath[31,32], K. Márton, A.J. Rádl[33], F. Sikler, V. Veszpremi

MTA-ELTE Lendület CMS Particle and Nuclear Physics Group, Eötvös Loránd University, Budapest, Hungary
M. Csanád, K. Farkas, A. Fehérkuti[34], M.M.A. Gadallah[35], Á. Kadlecsik, P. Major, G. Pásztor, G.I. Veres

Faculty of Informatics, University of Debrecen, Debrecen, Hungary
P. Raics, B. Ujvari, G. Zilizi

Institute of Nuclear Research ATOMKI, Debrecen, Hungary
G. Bencze, S. Czellar, J. Molnar, Z. Szillasi

Karoly Robert Campus, MATE Institute of Technology, Gyongyos, Hungary
T. Csorgo[34], T. Novak

Panjab University, Chandigarh, India
J. Babbar, S. Bansal, S.B. Beri, V. Bhatnagar, G. Chaudhary, S. Chauhan, N. Dhingra[36], A. Kaur, A. Kaur, H. Kaur, M. Kaur, S. Kumar, K. Sandeep, T. Sheokand, J.B. Singh, A. Singla

University of Delhi, Delhi, India
A. Ahmed, A. Bhardwaj, A. Chhetri, B.C. Choudhary, A. Kumar, A. Kumar, M. Naimuddin, K. Ranjan, S. Saumya

Saha Institute of Nuclear Physics, HBNI, Kolkata, India
S. Baradia, S. Barman[37], S. Bhattacharya, S. Das Gupta, S. Dutta, S. Dutta, S. Sarkar

Indian Institute of Technology Madras, Madras, India
M.M. Ameen, P.K. Behera, S.C. Behera, S. Chatterjee, G. Dash, P. Jana, P. Kalbhor, S. Kamble, J.R. Komaragiri[38], D. Kumar[38], P.R. Pujahari, N.R. Saha, A. Sharma, A.K. Sikdar, R.K. Singh, P. Verma, S. Verma, A. Vijay

Tata Institute of Fundamental Research-A, Mumbai, India
S. Dugad, M. Kumar, G.B. Mohanty, B. Parida, M. Shelake, P. Suryadevara

Tata Institute of Fundamental Research-B, Mumbai, India
A. Bala, S. Banerjee, R.M. Chatterjee, M. Guchait, Sh. Jain, A. Jaiswal, S. Kumar, G. Majumder, K. Mazumdar, S. Parolia, A. Thachayath

National Institute of Science Education and Research, An OCC of Homi Bhabha National Institute, Bhubaneswar, Odisha, India
S. Bahinipati[39], C. Kar, D. Maity[40], P. Mal, T. Mishra, V.K. Muraleedharan Nair Bindhu[40], K. Naskar[40], A. Nayak[40], S. Nayak, K. Pal, P. Sadangi, S.K. Swain, S. Varghese[40], D. Vats[40]

Indian Institute of Science Education and Research (IISER), Pune, India
S. Acharya[41], A. Alpana, S. Dube, B. Gomber[41], P. Hazarika, B. Kansal, A. Laha, B. Sahu[41], S. Sharma, K.Y. Vaish

Isfahan University of Technology, Isfahan, Iran
H. Bakhshiansohi[42], A. Jafari[43], M. Zeinali[44]

Institute for Research in Fundamental Sciences (IPM), Tehran, Iran
S. Bashiri, S. Chenarani[45], S.M. Etesami, Y. Hosseini, M. Khakzad, E. Khazaie[46], M. Mohammadi Najafabadi, S. Tizchang

University College Dublin, Dublin, Ireland
M. Felcini, M. Grunewald

INFN Sezione di Bari[a], Università di Bari[b], Politecnico di Bari[c], Bari, Italy
M. Abbrescia[a,b], A. Colaleo[a,b], D. Creanza[a,c], B. D'Anzi[a,b], N. De Filippis[a,c], M. De Palma[a,b], A. Di Florio[a,c], L. Fiore[a], G. Iaselli[a,c], M. Louka[a,b], G. Maggi[a,c], M. Maggi[a], I. Margjeka[a,b], V. Mastrapasqua[a,b], S. My[a,b], S. Nuzzo[a,b], A. Pellecchia[a,b], A. Pompili[a,b], G. Pugliese[a,c], R. Radogna[a], D. Ramos[a], A. Ranieri[a], L. Silvestris[a], F.M. Simone[a,b], Ü. Sözbilir[a], A. Stamerra[a], D. Troiano[a], R. Venditti[a], P. Verwilligen[a], A. Zaza[a,b]

INFN Sezione di Bologna[a], Università di Bologna[b], Bologna, Italy
G. Abbiendi[a], C. Battilana[a,b], D. Bonacorsi[a,b], L. Borgonovi[a], P. Capiluppi[a,b], A. Castro[a,b], F.R. Cavallo[a], M. Cuffiani[a,b], G.M. Dallavalle[a], T. Diotalevi[a,b], F. Fabbri[a], A. Fanfani[a,b], D. Fasanella[a,b], P. Giacomelli[a], L. Giommi[a,b], C. Grandi[a], L. Guiducci[a,b], S. Lo Meo[a,47], M. Lorusso[a,b], L. Lunerti[a], S. Marcellini[a], G. Masetti[a], F.L. Navarria[a,b], G. Paggi[a], A. Perrotta[a], F. Primavera[a,b], A.M. Rossi[a,b], S. Rossi Tisbeni[a,b], T. Rovelli[a,b], G.P. Siroli[a,b]

INFN Sezione di Catania[a], Università di Catania[b], Catania, Italy
S. Costa[a,b,48], A. Di Mattia[a], R. Potenza[a,b], A. Tricomi[a,b,48], C. Tuve[a,b]

INFN Sezione di Firenze[a], Università di Firenze[b], Firenze, Italy
P. Assiouras[a], G. Barbagli[a], G. Bardelli[a,b], B. Camaiani[a,b], A. Cassese[a], R. Ceccarelli[a], V. Ciulli[a,b], C. Civinini[a], R. D'Alessandro[a,b], E. Focardi[a,b], T. Kello[a], G. Latino[a,b], P. Lenzi[a,b], M. Lizzo[a], M. Meschini[a], S. Paoletti[a], A. Papanastassiou[a,b], G. Sguazzoni[a], L. Viliani[a]

INFN Laboratori Nazionali di Frascati, Frascati, Italy
L. Benussi, S. Bianco, S. Meola[49], D. Piccolo

INFN Sezione di Genova[a], Università di Genova[b], Genova, Italy
P. Chatagnon[a], F. Ferro[a], E. Robutti[a], S. Tosi[a,b]

INFN Sezione di Milano-Bicocca[a], Università di Milano-Bicocca[b], Milano, Italy
A. Benaglia[a], G. Boldrini[a,b], F. Brivio[a], F. Cetorelli[a], F. De Guio[a,b], M.E. Dinardo[a,b], P. Dini[a], S. Gennai[a], R. Gerosa[a,b], A. Ghezzi[a,b], P. Govoni[a,b], L. Guzzi[a], M.T. Lucchini[a,b], M. Malberti[a], S. Malvezzi[a], A. Massironi[a], D. Menasce[a], L. Moroni[a], M. Paganoni[a,b], S. Palluotto[a,b], D. Pedrini[a], A. Perego[a], B.S. Pinolini[a], G. Pizzati[a,b], S. Ragazzi[a,b], T. Tabarelli de Fatis[a,b]

INFN Sezione di Napoli[a], Università di Napoli 'Federico II'[b], Napoli, Italy; Università della Basilicata[c], Potenza, Italy; Scuola Superiore Meridionale (SSM)[d], Napoli, Italy
S. Buontempo[a], A. Cagnotta[a,b], F. Carnevali[a,b], N. Cavallo[a,c], F. Fabozzi[a,c], A.O.M. Iorio[a,b], L. Lista[a,b,50], P. Paolucci[a,29], B. Rossi[a], C. Sciacca[a,b]

INFN Sezione di Padova[a], Università di Padova[b], Padova, Italy; Università di Trento[c], Trento, Italy
R. Ardino[a], P. Azzi[a], N. Bacchetta[a,51], P. Bortignon[a], G. Bortolato[a,b], A. Bragagnolo[a,b], A.C.M. Bulla[a], R. Carlin[a,b], P. Checchia[a], T. Dorigo[a], F. Gasparini[a,b], U. Gasparini[a,b], E. Lusiani[a], M. Margoni[a,b], A.T. Meneguzzo[a,b], M. Migliorini[a,b], F. Montecassiano[a], M. Passaseo[a], J. Pazzini[a,b], P. Ronchese[a,b], R. Rossin[a,b], F. Simonetto[a,b], G. Strong[a], M. Tosi[a,b], A. Triossi[a,b], S. Ventura[a], P. Zotto[a,b], A. Zucchetta[a,b], G. Zumerle[a,b]

INFN Sezione di Pavia[a], Università di Pavia[b], Pavia, Italy
C. Aimè[a], A. Braghieri[a], S. Calzaferri[a], D. Fiorina[a], P. Montagna[a,b], V. Re[a], C. Riccardi[a,b], P. Salvini[a], I. Vai[a,b], P. Vitulo[a,b]

INFN Sezione di Perugia[a], Università di Perugia[b], Perugia, Italy
S. Ajmal[a,b], M.E. Ascioti[a,b], G.M. Bilei[a], C. Carrivale[a,b], D. Ciangottini[a,b], L. Fanò[a,b], M. Magherini[a,b], V. Mariani[a,b], M. Menichelli[a], F. Moscatelli[a,52], A. Rossi[a,b], A. Santocchia[a,b], D. Spiga[a], T. Tedeschi[a,b]

INFN Sezione di Pisa[a], Università di Pisa[b], Scuola Normale Superiore di Pisa[c], Pisa, Italy; Università di Siena[d], Siena, Italy
C.A. Alexe[a,c], P. Asenov[a,b], P. Azzurri[a], G. Bagliesi[a], R. Bhattacharya[a], L. Bianchini[a,b], T. Boccali[a], E. Bossini[a], D. Bruschini[a,c], R. Castaldi[a], M.A. Ciocci[a,b], M. Cipriani[a,b], V. D'Amante[a,d], R. Dell'Orso[a], S. Donato[a], A. Giassi[a], F. Ligabue[a,c], D. Matos Figueiredo[a], A. Messineo[a,b], M. Musich[a,b], F. Palla[a], A. Rizzi[a,b], G. Rolandi[a,c], S. Roy Chowdhury[a], T. Sarkar[a], A. Scribano[a], P. Spagnolo[a], R. Tenchini[a], G. Tonelli[a,b], N. Turini[a,d], F. Vaselli[a,c], A. Venturi[a], P.G. Verdini[a]

INFN Sezione di Roma[a], Sapienza Università di Roma[b], Roma, Italy
C. Baldenegro Barrera[a,b], P. Barria[a], C. Basile[a,b], M. Campana[a,b], F. Cavallari[a], L. Cunqueiro Mendez[a,b], D. Del Re[a,b], E. Di Marco[a], M. Diemoz[a], F. Errico[a,b], E. Longo[a,b], P. Meridiani[a], J. Mijuskovic[a,b], G. Organtini[a,b], F. Pandolfi[a], R. Paramatti[a,b], C. Quaranta[a,b], S. Rahatlou[a,b], C. Rovelli[a], F. Santanastasio[a,b], L. Soffi[a]

INFN Sezione di Torino[a], Università di Torino[b], Torino, Italy; Università del Piemonte Orientale[c], Novara, Italy
N. Amapane[a,b], R. Arcidiacono[a,c], S. Argiro[a,b], M. Arneodo[a,c], N. Bartosik[a], R. Bellan[a,b], A. Bellora[a,b], C. Biino[a], C. Borca[a,b], N. Cartiglia[a], M. Costa[a,b], R. Covarelli[a,b], N. Demaria[a], L. Finco[a], M. Grippo[a,b], B. Kiani[a,b], F. Legger[a], F. Luongo[a,b], C. Mariotti[a], L. Markovic[a,b], S. Maselli[a], A. Mecca[a,b], L. Menzio[a,b],

E. Migliore[a,b], M. Monteno[a], R. Mulargia[a], M.M. Obertino[a,b], G. Ortona[a], L. Pacher[a,b], N. Pastrone[a], M. Pelliccioni[a], M. Ruspa[a,c], F. Siviero[a,b], V. Sola[a,b], A. Solano[a,b], A. Staiano[a], C. Tarricone[a,b], D. Trocino[a], G. Umoret[a,b], E. Vlasov[a,b], R. White[a,b]

INFN Sezione di Trieste[a], Università di Trieste[b], Trieste, Italy
S. Belforte[a], V. Candelise[a,b], M. Casarsa[a], F. Cossutti[a], K. De Leo[a], G. Della Ricca[a,b]

Kyungpook National University, Daegu, Korea
S. Dogra, J. Hong, C. Huh, B. Kim, J. Kim, D. Lee, H. Lee, S.W. Lee, C.S. Moon, Y.D. Oh, M.S. Ryu, S. Sekmen, B. Tae, Y.C. Yang

Department of Mathematics and Physics - GWNU, Gangneung, Korea
M.S. Kim

Chonnam National University, Institute for Universe and Elementary Particles, Kwangju, Korea
G. Bak, P. Gwak, H. Kim, D.H. Moon

Hanyang University, Seoul, Korea
E. Asilar, J. Choi, D. Kim, T.J. Kim, J.A. Merlin, Y. Ryou

Korea University, Seoul, Korea
S. Choi, S. Han, B. Hong, K. Lee, K.S. Lee, S. Lee, S.K. Park, J. Yoo

Kyung Hee University, Department of Physics, Seoul, Korea
J. Goh, S. Yang

Sejong University, Seoul, Korea
H. S. Kim, Y. Kim, S. Lee

Seoul National University, Seoul, Korea
J. Almond, J.H. Bhyun, J. Choi, J. Choi, W. Jun, J. Kim, S. Ko, H. Kwon, H. Lee, J. Lee, J. Lee, B.H. Oh, S.B. Oh, H. Seo, U.K. Yang, I. Yoon

University of Seoul, Seoul, Korea
W. Jang, D.Y. Kang, Y. Kang, S. Kim, B. Ko, J.S.H. Lee, Y. Lee, I.C. Park, Y. Roh, I.J. Watson

Yonsei University, Department of Physics, Seoul, Korea
S. Ha, H.D. Yoo

Sungkyunkwan University, Suwon, Korea
M. Choi, M.R. Kim, H. Lee, Y. Lee, I. Yu

College of Engineering and Technology, American University of the Middle East (AUM), Dasman, Kuwait
T. Beyrouthy

Riga Technical University, Riga, Latvia
K. Dreimanis, A. Gaile, G. Pikurs, A. Potrebko, M. Seidel, D. Sidiropoulos Kontos

University of Latvia (LU), Riga, Latvia
N.R. Strautnieks

Vilnius University, Vilnius, Lithuania

M. Ambrozas, A. Juodagalvis, A. Rinkevicius, G. Tamulaitis

National Centre for Particle Physics, Universiti Malaya, Kuala Lumpur, Malaysia
N. Bin Norjoharuddeen, I. Yusuff[53], Z. Zolkapli

Universidad de Sonora (UNISON), Hermosillo, Mexico
J.F. Benitez, A. Castaneda Hernandez, H.A. Encinas Acosta, L.G. Gallegos Maríñez, M. León Coello, J.A. Murillo Quijada, A. Sehrawat, L. Valencia Palomo

Centro de Investigacion y de Estudios Avanzados del IPN, Mexico City, Mexico
G. Ayala, H. Castilla-Valdez, H. Crotte Ledesma, E. De La Cruz-Burelo, I. Heredia-De La Cruz[54], R. Lopez-Fernandez, J. Mejia Guisao, C.A. Mondragon Herrera, A. Sánchez Hernández

Universidad Iberoamericana, Mexico City, Mexico
C. Oropeza Barrera, D.L. Ramirez Guadarrama, M. Ramírez García

Benemerita Universidad Autonoma de Puebla, Puebla, Mexico
I. Bautista, I. Pedraza, H.A. Salazar Ibarguen, C. Uribe Estrada

University of Montenegro, Podgorica, Montenegro
I. Bubanja, N. Raicevic

University of Canterbury, Christchurch, New Zealand
P.H. Butler

National Centre for Physics, Quaid-I-Azam University, Islamabad, Pakistan
A. Ahmad, M.I. Asghar, A. Awais, M.I.M. Awan, H.R. Hoorani, W.A. Khan

AGH University of Krakow, Faculty of Computer Science, Electronics and Telecommunications, Krakow, Poland
V. Avati, L. Grzanka, M. Malawski

National Centre for Nuclear Research, Swierk, Poland
H. Bialkowska, M. Bluj, M. Górski, M. Kazana, M. Szleper, P. Zalewski

Institute of Experimental Physics, Faculty of Physics, University of Warsaw, Warsaw, Poland
K. Bunkowski, K. Doroba, A. Kalinowski, M. Konecki, J. Krolikowski, A. Muhammad

Warsaw University of Technology, Warsaw, Poland
K. Pozniak, W. Zabolotny

Laboratório de Instrumentação e Física Experimental de Partículas, Lisboa, Portugal
M. Araujo, D. Bastos, C. Beirão Da Cruz E Silva, A. Boletti, M. Bozzo, T. Camporesi, G. Da Molin, P. Faccioli, M. Gallinaro, J. Hollar, N. Leonardo, G.B. Marozzo, T. Niknejad, A. Petrilli, M. Pisano, J. Seixas, J. Varela, J.W. Wulff

Faculty of Physics, University of Belgrade, Belgrade, Serbia
P. Adzic, P. Milenovic

VINCA Institute of Nuclear Sciences, University of Belgrade, Belgrade, Serbia
M. Dordevic, J. Milosevic, L. Nadderd, V. Rekovic

Centro de Investigaciones Energéticas Medioambientales y Tecnológicas (CIEMAT), Madrid, Spain
J. Alcaraz Maestre, Cristina F. Bedoya, Oliver M. Carretero, M. Cepeda,

M. Cerrada, N. Colino, B. De La Cruz, A. Delgado Peris, A. Escalante Del Valle, D. Fernández Del Val, J.P. Fernández Ramos, J. Flix, M.C. Fouz, O. Gonzalez Lopez, S. Goy Lopez, J.M. Hernandez, M.I. Josa, D. Moran, C. M. Morcillo Perez, Á. Navarro Tobar, C. Perez Dengra, A. Pérez-Calero Yzquierdo, J. Puerta Pelayo, I. Redondo, S. Sánchez Navas, J. Sastre, L. Urda Gómez, J. Vazquez Escobar

Universidad Autónoma de Madrid, Madrid, Spain
J.F. de Trocóniz

Universidad de Oviedo, Instituto Universitario de Ciencias y Tecnologías Espaciales de Asturias (ICTEA), Oviedo, Spain
B. Alvarez Gonzalez, J. Cuevas, J. Fernandez Menendez, S. Folgueras, I. Gonzalez Caballero, J.R. González Fernández, P. Leguina, E. Palencia Cortezon, C. Ramón Álvarez, V. Rodríguez Bouza, A. Soto Rodríguez, A. Trapote, C. Vico Villalba, P. Vischia

Instituto de Física de Cantabria (IFCA), CSIC-Universidad de Cantabria, Santander, Spain
S. Bhowmik, S. Blanco Fernández, J.A. Brochero Cifuentes, I.J. Cabrillo, A. Calderon, J. Duarte Campderros, M. Fernandez, G. Gomez, C. Lasaosa García, R. Lopez Ruiz, C. Martinez Rivero, P. Martinez Ruiz del Arbol, F. Matorras, P. Matorras Cuevas, E. Navarrete Ramos, J. Piedra Gomez, L. Scodellaro, I. Vila, J.M. Vizan Garcia

University of Colombo, Colombo, Sri Lanka
B. Kailasapathy[55], D.D.C. Wickramarathna

University of Ruhuna, Department of Physics, Matara, Sri Lanka
W.G.D. Dharmaratna[56], K. Liyanage, N. Perera

CERN, European Organization for Nuclear Research, Geneva, Switzerland
D. Abbaneo, C. Amendola, E. Auffray, G. Auzinger, J. Baechler, D. Barney, A. Bermúdez Martínez, M. Bianco, B. Bilin, A.A. Bin Anuar, A. Bocci, C. Botta, E. Brondolin, C. Caillol, G. Cerminara, N. Chernyavskaya, D. d'Enterria, A. Dabrowski, A. David, A. De Roeck, M.M. Defranchis, M. Deile, M. Dobson, G. Franzoni, W. Funk, S. Giani, D. Gigi, K. Gill, F. Glege, L. Gouskos, J. Hegeman, J.K. Heikkilä, B. Huber, V. Innocente, T. James, P. Janot, O. Kaluzinska, S. Laurila, P. Lecoq, E. Leutgeb, C. Lourenço, L. Malgeri, M. Mannelli, M. Matthewman, A. Mehta, F. Meijers, S. Mersi, E. Meschi, V. Milosevic, F. Monti, F. Moortgat, M. Mulders, I. Neutelings, S. Orfanelli, F. Pantaleo, G. Petrucciani, A. Pfeiffer, M. Pierini, H. Qu, D. Rabady, B. Ribeiro Lopes, M. Rovere, H. Sakulin, S. Sanchez Cruz, S. Scarfi, C. Schwick, M. Selvaggi, A. Sharma, K. Shchelina, P. Silva, P. Sphicas[57], A.G. Stahl Leiton, A. Steen, S. Summers, D. Treille, P. Tropea, D. Walter, J. Wanczyk[58], J. Wang, S. Wuchterl, P. Zehetner, P. Zejdl, W.D. Zeuner

Paul Scherrer Institut, Villigen, Switzerland
T. Bevilacqua[59], L. Caminada[59], A. Ebrahimi, W. Erdmann, R. Horisberger, Q. Ingram, H.C. Kaestli, D. Kotlinski, C. Lange, M. Missiroli[59], L. Noehte[59], T. Rohe

ETH Zurich - Institute for Particle Physics and Astrophysics (IPA), Zurich, Switzerland
T.K. Aarrestad, K. Androsov[58], M. Backhaus, G. Bonomelli, A. Calandri, C. Cazzaniga, K. Datta, P. De Bryas Dexmiers D'archiac[58], A. De Cosa, G. Dissertori,

M. Dittmar, M. Donegà, F. Eble, M. Galli, K. Gedia, F. Glessgen, C. Grab, N. Härringer, T.G. Harte, D. Hits, W. Lustermann, A.-M. Lyon, R.A. Manzoni, M. Marchegiani, L. Marchese, C. Martin Perez, A. Mascellani[58], F. Nessi-Tedaldi, F. Pauss, V. Perovic, S. Pigazzini, C. Reissel, T. Reitenspiess, B. Ristic, F. Riti, R. Seidita, J. Steggemann[58], D. Valsecchi, R. Wallny

Universität Zürich, Zurich, Switzerland
C. Amsler[60], P. Bärtschi, M.F. Canelli, K. Cormier, M. Huwiler, W. Jin, A. Jofrehei, B. Kilminster, S. Leontsinis, S.P. Liechti, A. Macchiolo, P. Meiring, F. Meng, U. Molinatti, J. Motta, A. Reimers, P. Robmann, M. Senger, E. Shokr, F. Stäger, R. Tramontano

National Central University, Chung-Li, Taiwan
C. Adloff[61], D. Bhowmik, C.M. Kuo, W. Lin, P.K. Rout, P.C. Tiwari[38], S.S. Yu

National Taiwan University (NTU), Taipei, Taiwan
L. Ceard, K.F. Chen, P.s. Chen, Z.g. Chen, A. De Iorio, W.-S. Hou, T.h. Hsu, Y.w. Kao, S. Karmakar, G. Kole, Y.y. Li, R.-S. Lu, E. Paganis, X.f. Su, J. Thomas-Wilsker, L.s. Tsai, H.y. Wu, E. Yazgan

High Energy Physics Research Unit, Department of Physics, Faculty of Science, Chulalongkorn University, Bangkok, Thailand
C. Asawatangtrakuldee, N. Srimanobhas, V. Wachirapusitanand

Çukurova University, Physics Department, Science and Art Faculty, Adana, Turkey
D. Agyel, F. Boran, F. Dolek, I. Dumanoglu[62], E. Eskut, Y. Guler[63], E. Gurpinar Guler[63], C. Isik, O. Kara, A. Kayis Topaksu, U. Kiminsu, G. Onengut, K. Ozdemir[64], A. Polatoz, B. Tali[65], U.G. Tok, S. Turkcapar, E. Uslan, I.S. Zorbakir

Middle East Technical University, Physics Department, Ankara, Turkey
G. Sokmen, M. Yalvac[66]

Bogazici University, Istanbul, Turkey
B. Akgun, I.O. Atakisi, E. Gülmez, M. Kaya[67], O. Kaya[68], S. Tekten[69]

Istanbul Technical University, Istanbul, Turkey
A. Cakir, K. Cankocak[62,70], G.G. Dincer[62], Y. Komurcu, S. Sen[71]

Istanbul University, Istanbul, Turkey
O. Aydilek[72], V. Epshteyn, B. Hacisahinoglu, I. Hos[73], B. Kaynak, S. Ozkorucuklu, O. Potok, H. Sert, C. Simsek, C. Zorbilmez

Yildiz Technical University, Istanbul, Turkey
S. Cerci[65], B. Isildak[74], D. Sunar Cerci, T. Yetkin

Institute for Scintillation Materials of National Academy of Science of Ukraine, Kharkiv, Ukraine
A. Boyaryntsev, B. Grynyov

National Science Centre, Kharkiv Institute of Physics and Technology, Kharkiv, Ukraine
L. Levchuk

University of Bristol, Bristol, United Kingdom
D. Anthony, J.J. Brooke, A. Bundock, F. Bury, E. Clement, D. Cussans, H. Flacher, M. Glowacki, J. Goldstein, H.F. Heath, M.-L. Holmberg, L. Kreczko,

S. Paramesvaran, L. Robertshaw, S. Seif El Nasr-Storey, V.J. Smith, N. Stylianou[75], K. Walkingshaw Pass

Rutherford Appleton Laboratory, Didcot, United Kingdom
A.H. Ball, K.W. Bell, A. Belyaev[76], C. Brew, R.M. Brown, D.J.A. Cockerill, C. Cooke, A. Elliot, K.V. Ellis, K. Harder, S. Harper, J. Linacre, K. Manolopoulos, D.M. Newbold, E. Olaiya, D. Petyt, T. Reis, A.R. Sahasransu, G. Salvi, T. Schuh, C.H. Shepherd-Themistocleous, I.R. Tomalin, K.C. Whalen, T. Williams

Imperial College, London, United Kingdom
R. Bainbridge, P. Bloch, C.E. Brown, O. Buchmuller, V. Cacchio, C.A. Carrillo Montoya, G.S. Chahal[77], D. Colling, J.S. Dancu, I. Das, P. Dauncey, G. Davies, J. Davies, M. Della Negra, S. Fayer, G. Fedi, G. Hall, M.H. Hassanshahi, A. Howard, G. Iles, M. Knight, J. Langford, J. León Holgado, L. Lyons, A.-M. Magnan, S. Mallios, M. Mieskolainen, J. Nash[78], M. Pesaresi, P.B. Pradeep, B.C. Radburn-Smith, A. Richards, A. Rose, K. Savva, C. Seez, R. Shukla, A. Tapper, K. Uchida, G.P. Uttley, L.H. Vage, T. Virdee[29], M. Vojinovic, N. Wardle, D. Winterbottom

Brunel University, Uxbridge, United Kingdom
K. Coldham, J.E. Cole, A. Khan, P. Kyberd, I.D. Reid

Baylor University, Waco, Texas, USA
S. Abdullin, A. Brinkerhoff, B. Caraway, E. Collins, J. Dittmann, K. Hatakeyama, J. Hiltbrand, B. McMaster, J. Samudio, S. Sawant, C. Sutantawibul, J. Wilson

Catholic University of America, Washington, DC, USA
R. Bartek, A. Dominguez, C. Huerta Escamilla, A.E. Simsek, R. Uniyal, A.M. Vargas Hernandez

The University of Alabama, Tuscaloosa, Alabama, USA
B. Bam, A. Buchot Perraguin, R. Chudasama, S.I. Cooper, C. Crovella, S.V. Gleyzer, E. Pearson, C.U. Perez, P. Rumerio[79], E. Usai, R. Yi

Boston University, Boston, Massachusetts, USA
A. Akpinar, C. Cosby, G. De Castro, Z. Demiragli, C. Erice, C. Fangmeier, E. Fontanesi, D. Gastler, F. Golf, S. Jeon, J. O'cain, I. Reed, J. Rohlf, K. Salyer, D. Sperka, D. Spitzbart, I. Suarez, A. Tsatsos, A.G. Zecchinelli

Brown University, Providence, Rhode Island, USA
G. Benelli, X. Coubez[25], D. Cutts, M. Hadley, U. Heintz, J.M. Hogan[80], T. Kwon, G. Landsberg, K.T. Lau, D. Li, J. Luo, S. Mondal, M. Narain[†], N. Pervan, S. Sagir[81], F. Simpson, M. Stamenkovic, N. Venkatasubramanian, X. Yan, W. Zhang

University of California, Davis, Davis, California, USA
S. Abbott, J. Bonilla, C. Brainerd, R. Breedon, H. Cai, M. Calderon De La Barca Sanchez, M. Chertok, M. Citron, J. Conway, P.T. Cox, R. Erbacher, F. Jensen, O. Kukral, G. Mocellin, M. Mulhearn, W. Wei, Y. Yao, F. Zhang

University of California, Los Angeles, California, USA
M. Bachtis, R. Cousins, A. Datta, G. Flores Avila, J. Hauser, M. Ignatenko, M.A. Iqbal, T. Lam, E. Manca, A. Nunez Del Prado, D. Saltzberg, V. Valuev

University of California, Riverside, Riverside, California, USA

R. Clare, J.W. Gary, M. Gordon, G. Hanson, W. Si, S. Wimpenny[†]

University of California, San Diego, La Jolla, California, USA
A. Aportela, A. Arora, J.G. Branson, S. Cittolin, S. Cooperstein, D. Diaz, J. Duarte, L. Giannini, Y. Gu, J. Guiang, R. Kansal, V. Krutelyov, R. Lee, J. Letts, M. Masciovecchio, F. Mokhtar, S. Mukherjee, M. Pieri, M. Quinnan, B.V. Sathia Narayanan, V. Sharma, M. Tadel, E. Vourliotis, F. Würthwein, Y. Xiang, A. Yagil

University of California, Santa Barbara - Department of Physics, Santa Barbara, California, USA
A. Barzdukas, L. Brennan, C. Campagnari, K. Downham, C. Grieco, J. Incandela, J. Kim, A.J. Li, P. Masterson, H. Mei, J. Richman, S.N. Santpur, U. Sarica, R. Schmitz, F. Setti, J. Sheplock, D. Stuart, T.Á. Vámi, S. Wang, D. Zhang

California Institute of Technology, Pasadena, California, USA
A. Bornheim, O. Cerri, A. Latorre, J. Mao, H.B. Newman, G. Reales Gutiérrez, M. Spiropulu, J.R. Vlimant, C. Wang, S. Xie, R.Y. Zhu

Carnegie Mellon University, Pittsburgh, Pennsylvania, USA
J. Alison, S. An, M.B. Andrews, P. Bryant, M. Cremonesi, V. Dutta, T. Ferguson, T.A. Gómez Espinosa, A. Harilal, A. Kallil Tharayil, C. Liu, T. Mudholkar, S. Murthy, P. Palit, K. Park, M. Paulini, A. Roberts, A. Sanchez, W. Terrill

University of Colorado Boulder, Boulder, Colorado, USA
J.P. Cumalat, W.T. Ford, A. Hart, A. Hassani, G. Karathanasis, N. Manganelli, A. Perloff, C. Savard, N. Schonbeck, K. Stenson, K.A. Ulmer, S.R. Wagner, N. Zipper, D. Zuolo

Cornell University, Ithaca, New York, USA
J. Alexander, S. Bright-Thonney, X. Chen, D.J. Cranshaw, J. Fan, X. Fan, S. Hogan, P. Kotamnives, J. Monroy, M. Oshiro, J.R. Patterson, M. Reid, A. Ryd, J. Thom, P. Wittich, R. Zou

Fermi National Accelerator Laboratory, Batavia, Illinois, USA
M. Albrow, M. Alyari, O. Amram, G. Apollinari, A. Apresyan, L.A.T. Bauerdick, D. Berry, J. Berryhill, P.C. Bhat, K. Burkett, J.N. Butler, A. Canepa, G.B. Cerati, H.W.K. Cheung, F. Chlebana, G. Cummings, J. Dickinson, I. Dutta, V.D. Elvira, Y. Feng, J. Freeman, A. Gandrakota, Z. Gecse, L. Gray, D. Green, A. Grummer, S. Grünendahl, D. Guerrero, O. Gutsche, R.M. Harris, R. Heller, T.C. Herwig, J. Hirschauer, B. Jayatilaka, S. Jindariani, M. Johnson, U. Joshi, T. Klijnsma, B. Klima, K.H.M. Kwok, S. Lammel, D. Lincoln, R. Lipton, T. Liu, C. Madrid, K. Maeshima, C. Mantilla, D. Mason, P. McBride, P. Merkel, S. Mrenna, S. Nahn, J. Ngadiuba, D. Noonan, S. Norberg, V. Papadimitriou, N. Pastika, K. Pedro, C. Pena[82], F. Ravera, A. Reinsvold Hall[83], L. Ristori, M. Safdari, E. Sexton-Kennedy, N. Smith, A. Soha, L. Spiegel, S. Stoynev, J. Strait, L. Taylor, S. Tkaczyk, N.V. Tran, L. Uplegger, E.W. Vaandering, I. Zoi

University of Florida, Gainesville, Florida, USA
C. Aruta, P. Avery, D. Bourilkov, P. Chang, V. Cherepanov, R.D. Field, E. Koenig, M. Kolosova, J. Konigsberg, A. Korytov, K. Matchev, N. Menendez, G. Mitselmakher, K. Mohrman, A. Muthirakalayil Madhu, N. Rawal, S. Rosenzweig, Y. Takahashi, J. Wang

Florida State University, Tallahassee, Florida, USA
T. Adams, A. Al Kadhim, A. Askew, S. Bower, R. Habibullah, V. Hagopian, R. Hashmi, R.S. Kim, S. Kim, T. Kolberg, G. Martinez, H. Prosper, P.R. Prova, M. Wulansatiti, R. Yohay, J. Zhang

Florida Institute of Technology, Melbourne, Florida, USA
B. Alsufyani, M.M. Baarmand, S. Butalla, S. Das, T. Elkafrawy[84], M. Hohlmann, M. Rahmani, E. Yanes

University of Illinois Chicago, Chicago, USA, Chicago, USA
M.R. Adams, A. Baty, C. Bennett, R. Cavanaugh, R. Escobar Franco, O. Evdokimov, C.E. Gerber, M. Hawksworth, A. Hingrajiya, D.J. Hofman, J.h. Lee, D. S. Lemos, A.H. Merrit, C. Mills, S. Nanda, G. Oh, B. Ozek, D. Pilipovic, R. Pradhan, E. Prifti, T. Roy, S. Rudrabhatla, M.B. Tonjes, N. Varelas, M.A. Wadud, Z. Ye, J. Yoo

The University of Iowa, Iowa City, Iowa, USA
M. Alhusseini, D. Blend, K. Dilsiz[85], L. Emediato, G. Karaman, O.K. Köseyan, J.-P. Merlo, A. Mestvirishvili[86], O. Neogi, H. Ogul[87], Y. Onel, A. Penzo, C. Snyder, E. Tiras[88]

Johns Hopkins University, Baltimore, Maryland, USA
B. Blumenfeld, L. Corcodilos, J. Davis, A.V. Gritsan, L. Kang, S. Kyriacou, P. Maksimovic, M. Roguljic, J. Roskes, S. Sekhar, M. Swartz

The University of Kansas, Lawrence, Kansas, USA
A. Abreu, L.F. Alcerro Alcerro, J. Anguiano, S. Arteaga Escatel, P. Baringer, A. Bean, Z. Flowers, D. Grove, J. King, G. Krintiras, M. Lazarovits, C. Le Mahieu, J. Marquez, N. Minafra, M. Murray, M. Nickel, M. Pitt, S. Popescu[89], C. Rogan, C. Royon, R. Salvatico, S. Sanders, C. Smith, G. Wilson

Kansas State University, Manhattan, Kansas, USA
B. Allmond, R. Gujju Gurunadha, A. Ivanov, K. Kaadze, A. Kalogeropoulos, Y. Maravin, J. Natoli, D. Roy, G. Sorrentino

University of Maryland, College Park, Maryland, USA
A. Baden, A. Belloni, J. Bistany-riebman, Y.M. Chen, S.C. Eno, N.J. Hadley, S. Jabeen, R.G. Kellogg, T. Koeth, B. Kronheim, Y. Lai, S. Lascio, A.C. Mignerey, S. Nabili, C. Palmer, C. Papageorgakis, M.M. Paranjpe, L. Wang

Massachusetts Institute of Technology, Cambridge, Massachusetts, USA
J. Bendavid, I.A. Cali, P.c. Chou, M. D'Alfonso, J. Eysermans, C. Freer, G. Gomez-Ceballos, M. Goncharov, G. Grosso, P. Harris, D. Hoang, D. Kovalskyi, J. Krupa, L. Lavezzo, Y.-J. Lee, K. Long, C. Mcginn, A. Novak, C. Paus, D. Rankin, C. Roland, G. Roland, S. Rothman, G.S.F. Stephans, Z. Wang, B. Wyslouch, T. J. Yang

University of Minnesota, Minneapolis, Minnesota, USA
B. Crossman, B.M. Joshi, C. Kapsiak, M. Krohn, D. Mahon, J. Mans, B. Marzocchi, M. Revering, R. Rusack, R. Saradhy, N. Strobbe

University of Mississippi, Oxford, Mississippi, USA
L.M. Cremaldi

University of Nebraska-Lincoln, Lincoln, Nebraska, USA

K. Bloom, D.R. Claes, G. Haza, J. Hossain, C. Joo, I. Kravchenko, J.E. Siado, W. Tabb, A. Vagnerini, A. Wightman, F. Yan, D. Yu

State University of New York at Buffalo, Buffalo, New York, USA
H. Bandyopadhyay, L. Hay, H.w. Hsia, I. Iashvili, A. Kharchilava, M. Morris, D. Nguyen, S. Rappoccio, H. Rejeb Sfar, A. Williams, P. Young

Northeastern University, Boston, Massachusetts, USA
G. Alverson, E. Barberis, J. Dervan, Y. Haddad, Y. Han, A. Krishna, J. Li, M. Lu, G. Madigan, R. Mccarthy, D.M. Morse, V. Nguyen, T. Orimoto, A. Parker, L. Skinnari, D. Wood

Northwestern University, Evanston, Illinois, USA
J. Bueghly, S. Dittmer, K.A. Hahn, Y. Liu, Y. Miao, D.G. Monk, M.H. Schmitt, A. Taliercio, M. Velasco

University of Notre Dame, Notre Dame, Indiana, USA
G. Agarwal, R. Band, R. Bucci, S. Castells, A. Das, R. Goldouzian, M. Hildreth, K.W. Ho, K. Hurtado Anampa, T. Ivanov, C. Jessop, K. Lannon, J. Lawrence, N. Loukas, L. Lutton, J. Mariano, N. Marinelli, I. Mcalister, T. McCauley, C. Mcgrady, C. Moore, Y. Musienko[17], H. Nelson, M. Osherson, A. Piccinelli, R. Ruchti, A. Townsend, Y. Wan, M. Wayne, H. Yockey, M. Zarucki, L. Zygala

The Ohio State University, Columbus, Ohio, USA
A. Basnet, B. Bylsma, M. Carrigan, L.S. Durkin, C. Hill, M. Joyce, M. Nunez Ornelas, K. Wei, B.L. Winer, B. R. Yates

Princeton University, Princeton, New Jersey, USA
H. Bouchamaoui, P. Das, G. Dezoort, P. Elmer, A. Frankenthal, B. Greenberg, N. Haubrich, K. Kennedy, G. Kopp, S. Kwan, D. Lange, A. Loeliger, D. Marlow, I. Ojalvo, J. Olsen, A. Shevelev, D. Stickland, C. Tully

University of Puerto Rico, Mayaguez, Puerto Rico, USA
S. Malik

Purdue University, West Lafayette, Indiana, USA
A.S. Bakshi, V.E. Barnes, S. Chandra, R. Chawla, A. Gu, L. Gutay, M. Jones, A.W. Jung, A.M. Koshy, M. Liu, G. Negro, N. Neumeister, G. Paspalaki, S. Piperov, V. Scheurer, J.F. Schulte, M. Stojanovic, J. Thieman, A. K. Virdi, F. Wang, W. Xie

Purdue University Northwest, Hammond, Indiana, USA
J. Dolen, N. Parashar, A. Pathak

Rice University, Houston, Texas, USA
D. Acosta, T. Carnahan, K.M. Ecklund, P.J. Fernández Manteca, S. Freed, P. Gardner, F.J.M. Geurts, W. Li, J. Lin, O. Miguel Colin, B.P. Padley, R. Redjimi, J. Rotter, E. Yigitbasi, Y. Zhang

University of Rochester, Rochester, New York, USA
A. Bodek, P. de Barbaro, R. Demina, J.L. Dulemba, A. Garcia-Bellido, O. Hindrichs, A. Khukhunaishvili, N. Parmar, P. Parygin[90], E. Popova[90], R. Taus

The Rockefeller University, New York, New York, USA
K. Goulianos

Rutgers, The State University of New Jersey, Piscataway, New Jersey, USA
B. Chiarito, J.P. Chou, S.V. Clark, D. Gadkari, Y. Gershtein, E. Halkiadakis, M. Heindl, C. Houghton, D. Jaroslawski, O. Karacheban[27], S. Konstantinou, I. Laflotte, A. Lath, R. Montalvo, K. Nash, J. Reichert, H. Routray, P. Saha, S. Salur, S. Schnetzer, S. Somalwar, R. Stone, S.A. Thayil, S. Thomas, J. Vora, H. Wang

University of Tennessee, Knoxville, Tennessee, USA
H. Acharya, D. Ally, A.G. Delannoy, S. Fiorendi, T. Holmes, A.R. Kanuganti, N. Karunarathna, L. Lee, E. Nibigira, S. Spanier

Texas A&M University, College Station, Texas, USA
D. Aebi, M. Ahmad, T. Akhter, O. Bouhali[91], R. Eusebi, J. Gilmore, T. Huang, T. Kamon[92], H. Kim, S. Luo, R. Mueller, D. Overton, D. Rathjens, A. Safonov

Texas Tech University, Lubbock, Texas, USA
N. Akchurin, J. Damgov, N. Gogate, V. Hegde, A. Hussain, Y. Kazhykarim, K. Lamichhane, S.W. Lee, A. Mankel, T. Peltola, I. Volobouev

Vanderbilt University, Nashville, Tennessee, USA
E. Appelt, Y. Chen, S. Greene, A. Gurrola, W. Johns, R. Kunnawalkam Elayavalli, A. Melo, F. Romeo, P. Sheldon, S. Tuo, J. Velkovska, J. Viinikainen

University of Virginia, Charlottesville, Virginia, USA
B. Cardwell, B. Cox, J. Hakala, R. Hirosky, A. Ledovskoy, C. Neu

Wayne State University, Detroit, Michigan, USA
S. Bhattacharya, P.E. Karchin

University of Wisconsin - Madison, Madison, Wisconsin, USA
A. Aravind, S. Banerjee, K. Black, T. Bose, S. Dasu, I. De Bruyn, P. Everaerts, C. Galloni, H. He, M. Herndon, A. Herve, C.K. Koraka, A. Lanaro, R. Loveless, J. Madhusudanan Sreekala, A. Mallampalli, A. Mohammadi, S. Mondal, G. Parida, L. Pétré, D. Pinna, A. Savin, V. Shang, V. Sharma, W.H. Smith, D. Teague, H.F. Tsoi, W. Vetens, A. Warden

Authors affiliated with an institute or an international laboratory covered by a cooperation agreement with CERN
S. Afanasiev, V. Alexakhin, V. Andreev, Yu. Andreev, T. Aushev, M. Azarkin, A. Babaev, A. Belyaev, V. Blinov[93], E. Boos, V. Borshch, D. Budkouski, V. Bunichev, V. Chekhovsky, R. Chistov[93], M. Danilov[93], A. Dermenev, T. Dimova[93], D. Druzhkin[94], M. Dubinin[82], L. Dudko, A. Ershov, G. Gavrilov, V. Gavrilov, S. Gninenko, V. Golovtcov, N. Golubev, I. Golutvin, I. Gorbunov, A. Gribushin, Y. Ivanov, V. Kachanov, V. Karjavine, A. Karneyeu, V. Kim[93], M. Kirakosyan, D. Kirpichnikov, M. Kirsanov, V. Klyukhin, O. Kodolova[95], D. Konstantinov, V. Korenkov, A. Kozyrev[93], N. Krasnikov, A. Lanev, P. Levchenko[96], N. Lychkovskaya, V. Makarenko, A. Malakhov, V. Matveev[93], V. Murzin, A. Nikitenko[97,95], S. Obraztsov, V. Oreshkin, V. Palichik, V. Perelygin, M. Perfilov, S. Petrushanko, S. Polikarpov[93], V. Popov, O. Radchenko[93], M. Savina, V. Savrin, V. Shalaev, S. Shmatov, S. Shulha, Y. Skovpen[93], S. Slabospitskii, V. Smirnov, D. Sosnov, V. Sulimov, E. Tcherniaev, A. Terkulov, O. Teryaev, I. Tlisova, A. Toropin, L. Uvarov, A. Uzunian, A. Vorobyev[†], N. Voytishin, B.S. Yuldashev[98], A. Zarubin, I. Zhizhin, A. Zhokin

†: Deceased
[1]Also at Yerevan State University, Yerevan, Armenia
[2]Also at TU Wien, Vienna, Austria
[3]Also at Institute of Basic and Applied Sciences, Faculty of Engineering, Arab Academy for Science, Technology and Maritime Transport, Alexandria, Egypt
[4]Also at Ghent University, Ghent, Belgium
[5]Also at Universidade do Estado do Rio de Janeiro, Rio de Janeiro, Brazil
[6]Also at Universidade Estadual de Campinas, Campinas, Brazil
[7]Also at Federal University of Rio Grande do Sul, Porto Alegre, Brazil
[8]Also at UFMS, Nova Andradina, Brazil
[9]Also at Nanjing Normal University, Nanjing, China
[10]Now at The University of Iowa, Iowa City, Iowa, USA
[11]Also at University of Chinese Academy of Sciences, Beijing, China
[12]Also at China Center of Advanced Science and Technology, Beijing, China
[13]Also at University of Chinese Academy of Sciences, Beijing, China
[14]Also at China Spallation Neutron Source, Guangdong, China
[15]Now at Henan Normal University, Xinxiang, China
[16]Also at Université Libre de Bruxelles, Bruxelles, Belgium
[17]Also at an institute or an international laboratory covered by a cooperation agreement with CERN
[18]Also at Suez University, Suez, Egypt
[19]Now at British University in Egypt, Cairo, Egypt
[20]Also at Purdue University, West Lafayette, Indiana, USA
[21]Also at Université de Haute Alsace, Mulhouse, France
[22]Also at Department of Physics, Tsinghua University, Beijing, China
[23]Also at The University of the State of Amazonas, Manaus, Brazil
[24]Also at University of Hamburg, Hamburg, Germany
[25]Also at RWTH Aachen University, III. Physikalisches Institut A, Aachen, Germany
[26]Also at Bergische University Wuppertal (BUW), Wuppertal, Germany
[27]Also at Brandenburg University of Technology, Cottbus, Germany
[28]Also at Forschungszentrum Jülich, Juelich, Germany
[29]Also at CERN, European Organization for Nuclear Research, Geneva, Switzerland
[30]Also at Institute of Physics, University of Debrecen, Debrecen, Hungary
[31]Also at Institute of Nuclear Research ATOMKI, Debrecen, Hungary
[32]Now at Universitatea Babes-Bolyai - Facultatea de Fizica, Cluj-Napoca, Romania
[33]Also at MTA-ELTE Lendület CMS Particle and Nuclear Physics Group, Eötvös Loránd University, Budapest, Hungary
[34]Also at HUN-REN Wigner Research Centre for Physics, Budapest, Hungary
[35]Also at Physics Department, Faculty of Science, Assiut University, Assiut, Egypt
[36]Also at Punjab Agricultural University, Ludhiana, India
[37]Also at University of Visva-Bharati, Santiniketan, India
[38]Also at Indian Institute of Science (IISc), Bangalore, India
[39]Also at IIT Bhubaneswar, Bhubaneswar, India
[40]Also at Institute of Physics, Bhubaneswar, India
[41]Also at University of Hyderabad, Hyderabad, India
[42]Also at Deutsches Elektronen-Synchrotron, Hamburg, Germany
[43]Also at Isfahan University of Technology, Isfahan, Iran
[44]Also at Sharif University of Technology, Tehran, Iran
[45]Also at Department of Physics, University of Science and Technology of Mazandaran,

Behshahr, Iran
[46]Also at Department of Physics, Isfahan University of Technology, Isfahan, Iran
[47]Also at Italian National Agency for New Technologies, Energy and Sustainable Economic Development, Bologna, Italy
[48]Also at Centro Siciliano di Fisica Nucleare e di Struttura Della Materia, Catania, Italy
[49]Also at Università degli Studi Guglielmo Marconi, Roma, Italy
[50]Also at Scuola Superiore Meridionale, Università di Napoli 'Federico II', Napoli, Italy
[51]Also at Fermi National Accelerator Laboratory, Batavia, Illinois, USA
[52]Also at Consiglio Nazionale delle Ricerche - Istituto Officina dei Materiali, Perugia, Italy
[53]Also at Department of Applied Physics, Faculty of Science and Technology, Universiti Kebangsaan Malaysia, Bangi, Malaysia
[54]Also at Consejo Nacional de Ciencia y Tecnología, Mexico City, Mexico
[55]Also at Trincomalee Campus, Eastern University, Sri Lanka, Nilaveli, Sri Lanka
[56]Also at Saegis Campus, Nugegoda, Sri Lanka
[57]Also at National and Kapodistrian University of Athens, Athens, Greece
[58]Also at Ecole Polytechnique Fédérale Lausanne, Lausanne, Switzerland
[59]Also at Universität Zürich, Zurich, Switzerland
[60]Also at Stefan Meyer Institute for Subatomic Physics, Vienna, Austria
[61]Also at Laboratoire d'Annecy-le-Vieux de Physique des Particules, IN2P3-CNRS, Annecy-le-Vieux, France
[62]Also at Near East University, Research Center of Experimental Health Science, Mersin, Turkey
[63]Also at Konya Technical University, Konya, Turkey
[64]Also at Izmir Bakircay University, Izmir, Turkey
[65]Also at Adiyaman University, Adiyaman, Turkey
[66]Also at Bozok Universitetesi Rektörlügü, Yozgat, Turkey
[67]Also at Marmara University, Istanbul, Turkey
[68]Also at Milli Savunma University, Istanbul, Turkey
[69]Also at Kafkas University, Kars, Turkey
[70]Now at stanbul Okan University, Istanbul, Turkey
[71]Also at Hacettepe University, Ankara, Turkey
[72]Also at Erzincan Binali Yildirim University, Erzincan, Turkey
[73]Also at Istanbul University - Cerrahpasa, Faculty of Engineering, Istanbul, Turkey
[74]Also at Yildiz Technical University, Istanbul, Turkey
[75]Also at Vrije Universiteit Brussel, Brussel, Belgium
[76]Also at School of Physics and Astronomy, University of Southampton, Southampton, United Kingdom
[77]Also at IPPP Durham University, Durham, United Kingdom
[78]Also at Monash University, Faculty of Science, Clayton, Australia
[79]Also at Università di Torino, Torino, Italy
[80]Also at Bethel University, St. Paul, Minnesota, USA
[81]Also at Karamanoğlu Mehmetbey University, Karaman, Turkey
[82]Also at California Institute of Technology, Pasadena, California, USA
[83]Also at United States Naval Academy, Annapolis, Maryland, USA
[84]Also at Ain Shams University, Cairo, Egypt
[85]Also at Bingol University, Bingol, Turkey
[86]Also at Georgian Technical University, Tbilisi, Georgia
[87]Also at Sinop University, Sinop, Turkey
[88]Also at Erciyes University, Kayseri, Turkey

[89]Also at Horia Hulubei National Institute of Physics and Nuclear Engineering (IFIN-HH), Bucharest, Romania
[90]Now at an institute or an international laboratory covered by a cooperation agreement with CERN
[91]Also at Texas A&M University at Qatar, Doha, Qatar
[92]Also at Kyungpook National University, Daegu, Korea
[93]Also at another institute or international laboratory covered by a cooperation agreement with CERN
[94]Also at Universiteit Antwerpen, Antwerpen, Belgium
[95]Also at Yerevan Physics Institute, Yerevan, Armenia
[96]Also at Northeastern University, Boston, Massachusetts, USA
[97]Also at Imperial College, London, United Kingdom
[98]Also at Institute of Nuclear Physics of the Uzbekistan Academy of Sciences, Tashkent, Uzbekistan